HAL
open science

A continuum mechanics model of enzyme-based tissue degradation in cancer therapies

Manon Deville, Roberto Natalini, Clair Poignard

To cite this version:

Manon Deville, Roberto Natalini, Clair Poignard. A continuum mechanics model of enzyme-based tissue degradation in cancer therapies. Bulletin of Mathematical Biology, In press, 10.1007/s11538-018-0515-2 . hal-01889575

HAL Id: hal-01889575

https://inria.hal.science/hal-01889575

Submitted on 7 Oct 2018

HAL is a multi-disciplinary open access archive for the deposit and dissemination of scientific research documents, whether they are published or not. The documents may come from teaching and research institutions in France or abroad, or from public or private research centers.

L'archive ouverte pluridisciplinaire **HAL**, est destinée au dépôt et à la diffusion de documents scientifiques de niveau recherche, publiés ou non, émanant des établissements d'enseignement et de recherche français ou étrangers, des laboratoires publics ou privés.

Bulletin of Mathematical Biology manuscript No.
(will be inserted by the editor)

A continuum mechanics model of enzyme-based tissue degradation in cancer therapies

Manon Deville · Roberto Natalini · Clair Poignard

Received: date / Accepted: date

Abstract We propose a mathematical model to describe enzyme-based tissue degradation in cancer therapies. The proposed model combines the poroelastic theory of mixtures with the transport of enzymes or drugs in the extracellular space. The effect of the matrix degrading enzymes on the tissue composition and its mechanical response are accounted for. Numerical simulations in 1D, 2D and axisymmetric (3D) configurations show how an injection of matrix degrading enzymes alters the porosity of a biological tissue. We eventually exhibit numerically the main consequences of a matrix degrading enzyme pretreatment in the framework of chemotherapy: the removal of the diffusive hindrance to the penetration of therapeutic molecules in tumors and the reduction of interstitial fluid pressure which improves transcapillary transport. Both effects are consistent with previous biological observations.

Keywords Mathematical biology · Poroelasticity · ECM degradation · Interstitial fluid pressure · Drug distribution in tissue

Mathematics Subject Classification (2000) 65M06, 65M12, 92C37

1 Introduction

1.1 Motivations

For several decades cancer research has developed a myriad of cytotoxic drugs, targeted therapies and immunotherapies to destroy or to control cancer tumors, with promising results. However these systemic therapies face the challenge of reaching the target tissue. These target tissues are either the tumor itself, which has to be reached by cytotoxic or targeted therapies, or the healthy organs such as muscles, which can generate a systemic immune response after specific plasmid transfection.
Whatever the final target –tumor or muscle– molecules have to cross multiple biological barriers, which stand between the drug at its site of administration and its ultimate target (Juliano 2007; Escoffre et al 2010). Consequently the optimization of therapeutic agent delivery has come to the research forefront in systemic cancer treatments.
Among the uptake of molecules in tissue, one can discriminate between the large molecules such as DNA plasmids and the small one like cytotoxic drugs. DNA plasmids are macromolecules which are used to

Manon Deville
Team MONC, INRIA Bordeaux-Sud-Ouest, Institut de Mathématiques de Bordeaux, CNRS UMR 5251 & Université de Bordeaux, 351 cours de la Libération, 33405 Talence Cedex, France
E-mail: manon.deville@inria.fr

Roberto Natalini
Istituto per le Applicazioni del Calcolo "M. Picone", Consiglio Nazionale delle Ricerche, Via dei Taurini 19, I-00185 Rome, Italy
E-mail: roberto.natalini@cnr.it

Clair Poignard Team MONC, INRIA Bordeaux-Sud-Ouest, Institut de Mathématiques de Bordeaux, CNRS UMR 5251 & Université de Bordeaux, 351 cours de la Libération, 33405 Talence Cedex, France
E-mail: clair.poignard@inria

generate an immune response in a muscle, in view of DNA cancer vaccination, while cytotoxic drugs are used to kill directly cancer cells.

DNA vaccination. The heuristics of DNA vaccination consist in injecting genetically engineered DNA plasmid so cells produce an antigen leading to a protective immunological response. So that plasmids cross the cell membranes, the gene transfection can be performed by mean of a virus or by means of a physical technique such as fluid pressure or electroporating electric field (Wolff et al 1990; André and Mir 2004; Leguèbe et al 2017). Viral and non viral DNA transfection face the issue of crossing the extracellular matrix (ECM) to reach the cell membranes, before being degraded by the extracellular nucleases (Bureau et al 2004).

Chemotherapy. The delivery of cytotoxic drugs to tumor cells occurs by diffusion and convection. The composition and structure of tumor-derived ECM can slow down the movement of therapeutic molecules within the tumor (Frantz et al 2010; Choi et al 2013; Minchinton and Tannock 2006). In addition, the disorganized vascular network and the absence of functional lymphatics in tumors diminished hydrostatic gradient from capillary to interstitium and thereby impaired exchanges of solutes over the capillary membranes (Bae et al 2013; Pietras et al 2001).

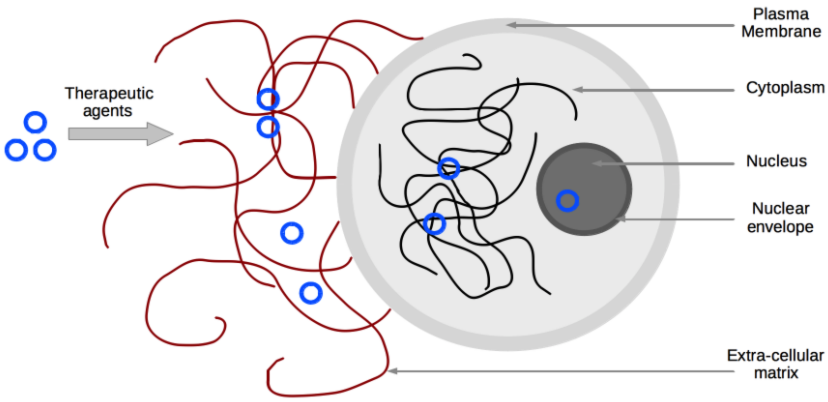

Fig. 1 After its injection into the target tissue, a therapeutic agent encounters biological barriers from extracellular environment toward the interior of the target cell.

The role of ECM degrading enzymes. The transport through the extracellular matrix is thus a critical step in drug delivery. ECM consists of a structural collagen network embedded in a gel of glycosaminoglycans (GAGs) and proteoglycans, which prevent the free diffusion of macromolecules such as DNA plasmids and slow down the free diffusion of cytotoxic drugs. Moreover, the anarchic tumor neovasculature combined with the tumor-derived ECM generates an interstitial fluid pressure (IFP) inside tumors, which prevent the drug delivery.
To overcome these drawbacks, it was proven that injecting an ECM degrading enzymes improves the molecule distribution. For exemple, regarding DNA transfection, the injection of hyaluronidase in muscles improves the DNA distribution within the tissue (Buhren et al 2016; Girish and Kemparaju 2007) leading to a better gene expression (Signori et al 2001; Akerstrom et al 2015; Schertzer et al 2006).
The use of ECM degrading enzymes in the vicinity of tumors have been controversial. For instance the hyaluronidase seems to be simultaneously a tumor promoter and a suppressor (Lokeshwar and Selzer 2008). In particular hyaluronidase alone could be a promoter of the metastatic spreading (McAtee et al 2014). However its combination with a cytotoxic drug seems to improve chemotherapy efficacy (Whatcott et al 2011). In particular, collagenase and hyaluronidase remove the diffusive hindrance to the penetration of therapeutic molecules in tumor models (Eikenes et al 2010; Ganesh et al 2008). Moreover

the intratumoral IFP is temporarily reduced by degrading the tumor ECM. Therefore collagenase and hyaluronidase improve the uptake and the distribution of cytotoxic molecules –and thus their efficacy– within solid tumors (Eikenes et al 2004, 2005; Brekken and de Lange Davies 1998).

Lack of numerical models. From the biological point of view, the effects of matrix degrading enzymes on drug transport is thus quite well understood. Their combination with cytotoxic molecules has been proven to improve the treatment efficacy, while their use as pretreatment in muscle improves the gene expression. However, the literature suffers from a lack of models describing the active transport of those enzymes in the extracellular medium and the resulting changes on the ECM. The aim of this paper is to provide a mathematical model that addresses this phenomenon in order to offer a better understanding of the physical involved phenomena.

1.2 Main results

The model consists of a non-linear system of partial differential equations (PDEs). It is derived directly from physical conservation laws. Constitutive relations are added to close the system. The derivation steps are presented in Figure 2. We adopt a poroelastic approach to model the mechanics of a biological tissue. This choice is made to take into account the swelling of the tissue when fluid is added by injection. It is also in accordance with the studies stating that biological tissue deformations are not negligible in numerical models describing drug delivery (Støverud et al 2011). This choice implies to first derive equations within the Eulerian formalism and then to reduce them to a fixed reference domain via a suitable change of variables in order to make the numerical processing possible. In addition, equations on the volume fractions of each component of the tissue are included to take the structural changes into account. In the end, the main variables of interest of the model are the three different volume fractions, the interstitial pressure, the displacement and the concentrations of enzyme and therapeutic agent respectively.
The final formulation of the model, system (54), is displayed in Section 3. To our knowledge, this is the first model describing the alteration of a poroelastic medium produced by chemical species injected directly in the medium. Alteration of a porous media is taken into account in (Alì et al 2007; Radu et al 2014) but within a rigid structure. Many mathematical models of passive transport into a poroelastic medium do not take into account exchanges between phases (Basser 1992; Støverud et al 2011; Chapelle and Moireau 2014). In (Fusi et al 2006; Lemon et al 2006; Sacco et al 2017), models including exchanges between phases are presented on closed poroelastic mixtures (no external sources or sinks). However, the changes are not mediated by external species. In (Spiegelman 1993a,b), magma is modeled as a poroelastic medium with varying porosity due to temperature changes. However, those changes are assumed to be infinitesimal. In (Chaplain et al 2006; Astanin and Preziosi 2008), poroelastic models taking into account ECM degradation by matrix degrading enzymes produced by tumor cells are presented within the particular framework of tumor growth. Nevertheless, these models have a very different focus, namely showing the formation of fibrosis. They also make slightly different assumptions: the ECM is rigid, the matrix degrading enzymes are produced by tumor cells and the cells movement is similar to an elastic fluid.
The goal of the paper is to derive a model that combines the effect of an injection of ECM degradation enzyme with a poroelastic macroscopic model of biological tissue (skeletal muscle or tumor tissue), and to provide a numerical method that allows to simulate the complete model in 1D-, 2D-, and axisymmetric configurations in order to compare the results with the qualitative data available in the litterature. Let us note that this paper provides the first step towards the long-term goal of the numerical optimization of drug delivery in tissues with enzyme pretreatment.

Numerical simulations illustrating biological phenomena. After testing the model with a set of numerical simulations to investigate the effect of the new parameters added (Figures 12 and 14), we use the model to describe two situations: the incubation of a spheroid into an ECM degradation enzyme and the intratumoral injection of enzyme in vivo. We observe that, in the first test case, given the dependency of the diffusion tensor on the porosity variable (Magzoub et al 2008), a pretreatment with ECM degradation enzyme affects the distribution of therapeutic agents, thereby improving the diffusion process. Where

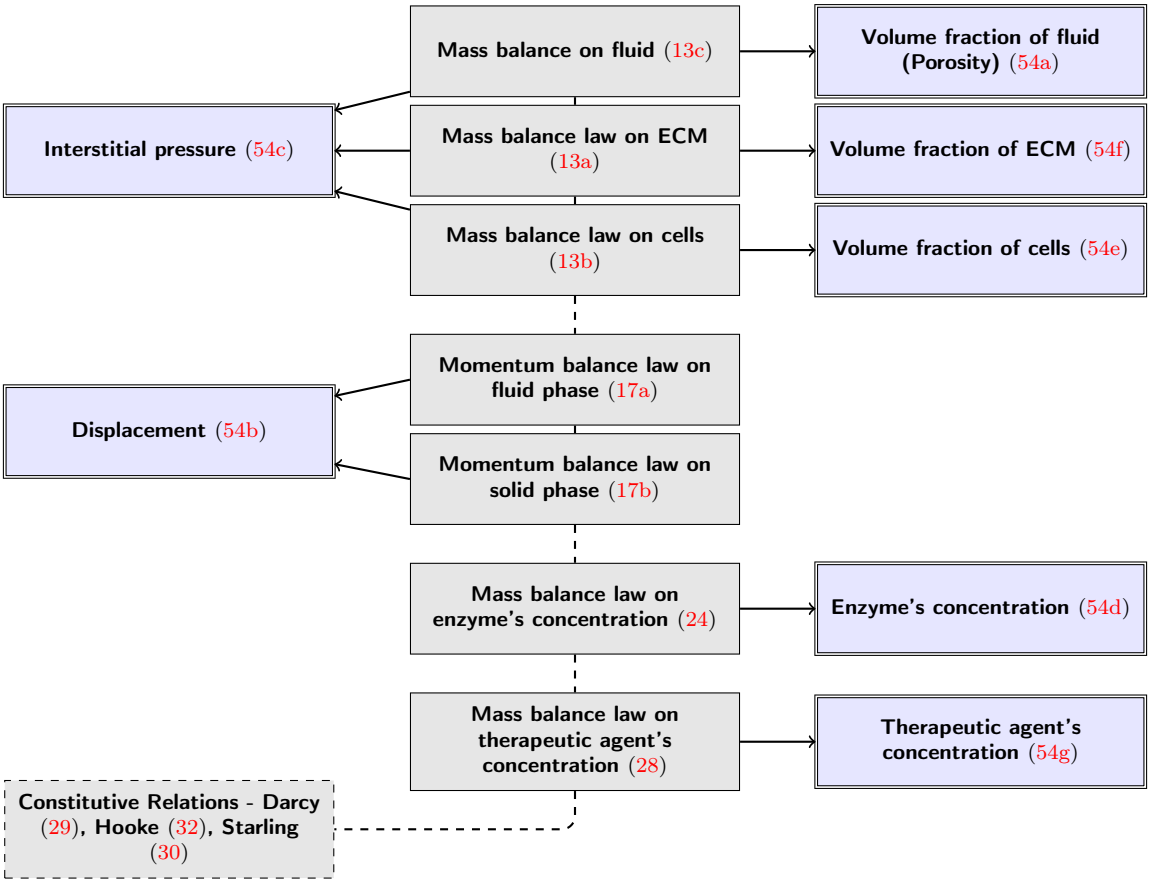

Fig. 2 Schematic description of the model derivation. The first set of boxes contains the set of conservation laws and constitutive relations considered while the other boxes contain the final equations on the variables of interest derived from the physical laws. The numbering refers to the corresponding equations in their final form stated further in the article.

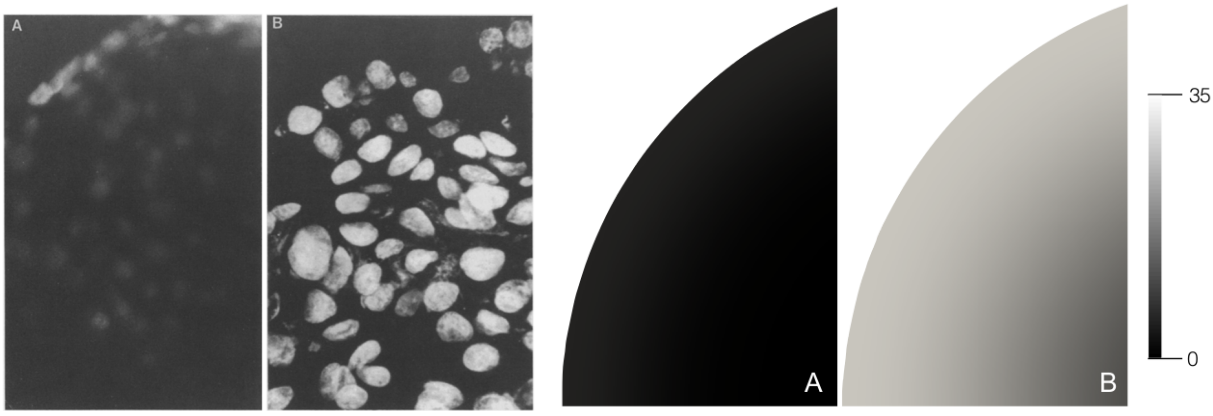

Fig. 3 Comparison between experimental doxuribicin fluorescence (left, data from (Kohno et al 1994)) and numerically simulated (see Figure 18 in Section 5) concentration of anticancer agent in a spheroid previously incubated with hyaluronidase (B) or not (A).

without pretreatment, the macromolecules stay mainly at the periphery of the spheroid, a pretreatment with hyaluronidase leads to a deeper distribution in the spheroid (Figure 3).

In the second case, given the dependency of the pressure on the porosity variable, an intratumoral injection of enzyme results in a reduction of the IFP. This reduction depends non monotonically on the enzyme concentration. Actually the IFP reduction reaches a maximum value for a certain dose of

hyaluronidase, while a further increase of the dose results in a smaller IFP reduction, which is qualitatively in accordance with the experiments (Figure 4).

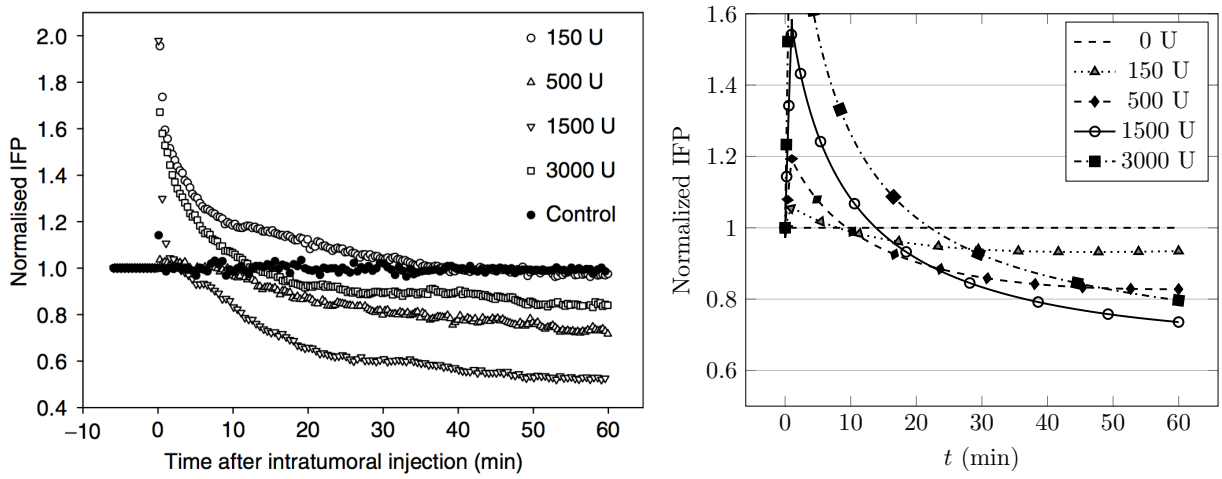

Fig. 4 Comparison between experimental IFP (left, data from (Eikenes et al 2005)) and numerically simulated IFP (see 5.3.4). Normalized interstitial fluid pressure is represented in both cases as a function of time after intratumoral injection of 150 U, 500 U, 1500 U and 3000 U hyaluronidase in tumors compared to no pretreatment (intratumoral injection of saline solution).

It also appears that a pretreatment with ECM degradation enzyme affects the distribution of therapeutic agents, thereby increasing its area of action by improving both the diffusion and the convection processes. This is once more in accordance with the experiments (data from (Eikenes et al 2005)). Indeed, without pretreatment, the macromolecules stay only at the periphery of the tumor, the transcapillary transport being greatly reduced by the high IFP inside the tumor. A pretreatment with hyaluronidase permit to obtain a wider distribution. The molecules are thus distributed all over the tumor (Figure 5).

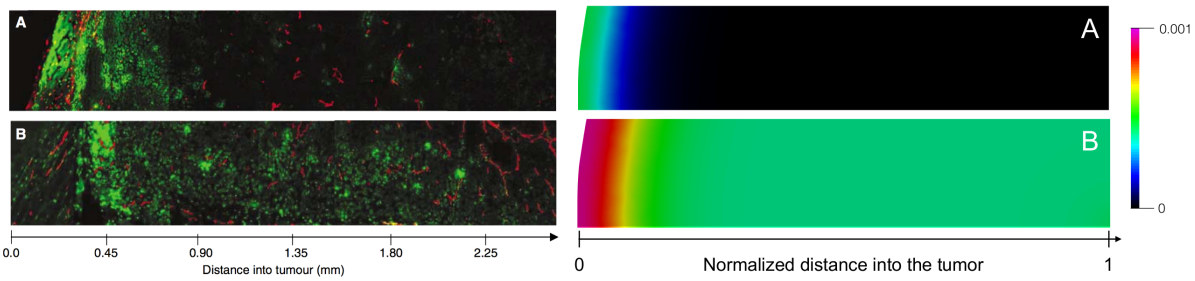

Fig. 5 Comparison between experimental distribution of anticancer fluorescent agent (left, data from (Eikenes et al 2005)) and numerically simulated concentration of agent. In case A, no pretreatment was previously performed on the tissue whereas in case B, the tissue was pretreated with 1500 U hyaluronidase.

1.3 Outline

In this paper, we construct a non-linear spatio-temporal model for the active transport of ECM degradation enzyme into a poroelastic biological tissue coupled with the passive transport of therapeutic agents. Section 2 is devoted to a precise description of our model following the scheme presented in Figure 2. It is divided in two parts: in the first part, we derive equations from physical conservation laws, while in the second part, we conclude the formulation of our model stating some constitutive relations. Section

3 is devoted to the simplification of the model. We formulate the equations of the model in a fixed Lagrangian domain and assume a small displacement hypothesis that simplifies the numerical processing. Section 4 contains the numerical scheme used to solve our PDE simplified model. The main features of the numerical model are then investigated in 1D- and 2D-configurations. We conclude by numerical simulations that corroborate experimental results in the framework of solid tumors in Section 5. To the best of our knowledge, it is the first time that a PDE model describes the effect of an injection of ECM degradation enzyme respectively on porosity, interstitial pressure and drug delivery.
It is worth noting that the use of the 3 phases: fluid, ECM and cell is essential to account for the main mechanisms involved in the transport of molecules. In particular, a simple model involving only the rigid solid constituents (ECM and cells) could not describe precisely the reduction of IFP thanks to the ECM degrading enzyme, which is transported by the fluid in the tissue. Therefore, despite its apparent complexity, the model presented in (54) is somehow the simplest physically relevant model to describe the coupling between the poroelastic description of 3–phase tissue and the influence of the ECM degrading enzyme on the tissue poroelasticity, which degrades by definition only the ECM phase.
Previous experiments performed by Professor Signori's team at the CNR Institute of Translational Pharmacology in Rome have exhibited the crucial importance of the hyaluronidase on the drug distribution as already shown in (Signori et al 2001). Moreover, tissue swelling is always reported in drug injection experiments, leading to an increase of the inner pressure, and thus to a nonzero drift force on the durg. All these experimental features show that simple reaction-diffusion systems cannot account precisely for the drug distribution when combined with ECM degrading enzymes.
It is also worth noting that our model involves many parameters, which can make it difficult to fit easily with biological experiments. To this end, and in order to propose optimized strategies for DNA transfection or cytotoxic drug distribution, we are developing a numerical strategy to calibrate and optimize the drug delivery in enzyme-based therapies. The premises of this forthcoming work based on kriging methods are described in (Deville 2017).

2 Derivation of the model

2.1 Framework

Modeling the behavior of porous media in which different continua interact at the microscopic level is not an easy task. In the current literature the mechanics of a porous medium is typically described by two different approaches: the averaging approach and the macroscopic approach (Ambrosi et al 2002), also known as mixture theory. The basic premise of the mixture theory is that the space occupied by a mixture is occupied co-jointly by the various constituents of the mixture, each considered as a continuum of its own. Thus, at any point of the space occupied by the mixture, there will be a particle belonging to each constituent (Fusi et al 2006). One can also cite the work of Chapelle and Moireau (Chapelle and Moireau 2014) for a rigorous general coupling of poroelastic flows with elasticity in an incompressible non-interacting 2-phase framework.
We let $\mathbf{x}$ and t denote the space and time variables, respectively. To simplify notations, we omit the dependence of all variables and model parameters on $\mathbf{x}$ and t, except otherwise stated.
We denote by $\Omega_0 = \Omega(0) \subset \mathbb{R}^d$ $(d = 1, 2, 3)$ the initial spatial configuration, by $\Omega_t = \Omega(t)$ the configuration at time t and by T the final time of the experiment.
The biological tissue is considered as a binary mixture of a solid and an interstitial fluid. The solid phase consists of cells and extracellular matrix (ECM). In what follows, the index ζ refers to one of the three constituents of the tissue: the fluid (f), the ECM $(\mathcal{E})$ or the cells $(\mathcal{C})$. The index s stands for the solid phase (ECM + cells). The density of the ζth constituent is denoted by ρ_ζ. It represents the mass of the ζth constituent per unit volume of the mixture. The density for the ζth constituent in a homogeneous state is denoted by ρ_ζ^R. It represents the mass of the ζth constituent per unit volume of the ζth constituent. The quantity defined by

$$\varphi_\zeta(t, \mathbf{x}) = \frac{\rho_\zeta(t, \mathbf{x})}{\rho_\zeta^R(t, \mathbf{x})}, \tag{1}$$

is the volume fraction of the mixture occupied by the ζth constituent. This definition coincides with the classic definition given by Bear and Bachmat (1990). The following standard assumptions on the mixture are considered.

Assumption 1 (**Saturation**) The mixture is fully saturated, i.e.

$$\varphi_{\mathcal{E}} + \varphi_{\mathscr{c}} + \varphi_f = 1 \qquad \forall \mathbf{x} \in \Omega, \;\; \forall t > 0 \tag{2}$$

This saturation condition excludes the possibility of the formation of voids or air bubbles inside the medium.

Assumption 2 (**Fluid incompressibility**) The liquid is incompressible in its pure state i.e. the density of the liquid in a homogeneous state is assumed to be a constant, namely

$$\rho_f^R(t,x) = \rho_f^{R,0}(t,x) \qquad \forall \mathbf{x} \in \Omega, \;\; \forall t > 0. \tag{3}$$

Assumption 3 All the solid matrix constituents (cells and ECM) have the same density in a homogeneous state:

$$\rho_{\mathcal{E}}^R(t,\mathbf{x}) = \rho_{\mathscr{c}}^R(t,\mathbf{x}) = \rho_s^R(t,\mathbf{x}). \tag{4}$$

Assumption 4 (**Slightly compressible solid**) The solid phase (ECM + cells) is slightly compressible in its pure state i.e. the density of the solid constituents in a homogeneous state can be written as (Chen et al 2006):

$$\rho_s^R(t,\mathbf{x}) = \rho_s^{R,0}(t,\mathbf{x})(1 + s_0(p(t,\mathbf{x}) - p(0,\mathbf{x}))), \qquad \forall \mathbf{x} \in \Omega, \;\; \forall t > 0, \tag{5}$$

where

$$s_0(p(t,\mathbf{x}) - p(0,\mathbf{x})) \ll 1, \qquad \forall \mathbf{x} \in \Omega, \;\; \forall t > 0, \tag{6}$$

and where p is the interstitial fluid pressure and where $\rho_s^{R,0}$ is a constant. s_0 can be related to the specific storage coefficient that appears in Biot's constitutive theory of consolidation (Biot 1941).

Assumption 5 (**Mass exchanges**) We assume that mass exchanges occur only among cells/ECM and fluid, meaning that degrading ECM is detoriated into extracellular fluid, and conversely that the latter is consumed whenever ECM is created.

Assumption 6 (**Fluid source term**) Fluid is exchanged between interstitial space and the blood or lymph vessels: the fluid source term is then assumed to be driven by the average transmural pressure. If fluid is directly injected in the tissue, another external source of fluid is added during the injection.

2.2 Balance laws

In this section we give the set of conservation laws that constitute our proposed mathematical picture of the mechanobiological properties of the tissue using the Eulerian formalism. All the solid matrix constituents (cells and ECM) are experiencing the same motion. Thus $\mathbf{v}_{\mathcal{E}}(t,\mathbf{x}) = \mathbf{v}_{\mathscr{c}}(t,\mathbf{x}) = \mathbf{v}_s(t,\mathbf{x})$. The motion function refers to the solid phase, so it is useful to use the Eulerian velocity of the fluid with respect to the solid phase defined by

$$\mathbf{w}(t,\mathbf{x}) = \mathbf{v}_f(t,\mathbf{x}) - \mathbf{v}_s(t,\mathbf{x}). \tag{7}$$

2.2.1 Mass balance for each component of the mixture

The mass of the ζth constituent can change due to

1. the flux caused by the motion at the velocity $\mathbf{v}_\zeta$ of the constituent,
2. the production that accounts for possible mass conversion between constituents at the specific rate Q_ζ (Fusi et al 2006),
3. the source term $\mathcal{S}_\zeta$.

One then has

$$\frac{\partial \rho_\zeta}{\partial t} + \nabla \cdot (\rho_\zeta \mathbf{v}_\zeta) - \rho_\zeta Q_\zeta - \mathcal{S}_\zeta = 0, \tag{8}$$

where the source term $\mathcal{S}_\zeta$ is given as

$$\mathcal{S}_\zeta = \rho_\zeta^R \Sigma_\zeta. \tag{9}$$

Using definition (1) we get

$$\frac{\partial(\rho_\zeta^R \varphi_\zeta)}{\partial t} + \nabla \cdot (\rho_\zeta^R \varphi_\zeta \mathbf{v}_\zeta) - \rho_\zeta^R \varphi_\zeta Q_\zeta - \mathcal{S}_\zeta = 0.$$

To translate Assumption 5, we assume the following constraint (Fusi et al 2006)

$$\rho_s^R \varphi_\mathcal{E} Q_\mathcal{E} + \rho_f^R \varphi_f Q_f = 0. \tag{10}$$

The production terms Q_f and $Q_\mathcal{E}$ introduced here describe the mechanisms of addition and/or removal of mass for each species constituting an isolated tissue. We assume that the ECM is degraded proportionally to the enzyme concentration (Altrock et al 2015), becoming fluid, and that the tissue recovers towards its initial physiological state.
It is then relevant to choose the production term $Q_\mathcal{E}$ as

$$Q_\mathcal{E} = -K\varphi_f c_{\text{enz}} + a_r \left(\varphi_f - \varphi_f^{\text{phys}}(\mathbf{x})\right). \tag{11}$$

where K is the rate of deterioration of the ECM when in contact with the enzyme, represented by its concentration in the fluid phase $\varphi_f c_{\text{enz}}$. The second term in the right hand side of expression of (11) represents the reconstitution of the tissue towards its physiological value φ_f^{phys} at the rate a_r as observed experimentally in (Juhlin. 1956; Happel et al 2014).
To translate Assumption 6, we choose the fluid source term as

$$\Sigma_f = Q_{\text{inj}}^{\text{tot}} + Q_{\text{vas}} - Q_{\text{lym}} \quad \text{where} \quad Q_{\text{inj}}^{\text{tot}} = Q_{\text{inj}}^{\text{enz}} + Q_{\text{inj}}^{\text{drug}}, \tag{12}$$

where $Q_{\text{inj}}^{\text{enz}}$ represents the injection term of enzyme, $Q_{\text{inj}}^{\text{drug}}$ represents the injection term of therapeutic agent, Q_{vas} is the transcapillary flow and Q_{lym} is the lymphatic drainage.
The mass balance equations for the tissue constituents are then expressed by the following coupled system of PDEs in $\Omega_t \times (0, T)$:

$$\begin{cases} \dfrac{\partial}{\partial t}(\rho_s^R \varphi_\mathcal{E}) + \nabla \cdot (\rho_s^R \varphi_\mathcal{E} \mathbf{v}_s) = \rho_s^R \varphi_\mathcal{E}(-K\varphi_f c_{\text{enz}} + a_r \left(\varphi_f - \varphi_f^{\text{phys}}\right)), & \text{(13a)} \\ \dfrac{\partial}{\partial t}(\rho_s^R \varphi_\mathscr{c}) + \nabla \cdot (\rho_s^R \varphi_\mathscr{c} \mathbf{v}_s) = 0, & \text{(13b)} \\ \dfrac{\partial}{\partial t}(\rho_f^R \varphi_f) + \nabla \cdot (\rho_f^R \varphi_f \mathbf{v}_f) = \rho_s^R \varphi_\mathcal{E} \left(K\varphi_f c_{\text{enz}} - a_r \left(\varphi_f - \varphi_f^{\text{phys}}\right)\right) + \rho_f^R (Q_{\text{inj}}^{\text{tot}} + Q_{\text{vas}} - Q_{\text{lym}}). & \text{(13c)} \end{cases}$$

2.2.2 Total mass balance for the mixture

Summing equations $(1/\rho_s^{R,0})\times$ (13a), $(1/\rho_s^{R,0})\times$ (13b) and $(1/\rho_f^R)\times$ (13c), using Assumptions 1 and 3, and conditions (6)-(10) we get

$$\begin{aligned} \varphi_s s_0 \left(\frac{\partial p}{\partial t} + \nabla p \cdot \mathbf{v}_s\right) + \nabla \cdot (\varphi_s \mathbf{v}_s + \varphi_f \mathbf{v}_f) &= Q_{\text{inj}}^{\text{tot}} + Q_{\text{vas}} - Q_{\text{lym}} \\ &+ \left(1 - \frac{\rho_s^{R,0}}{\rho_f^R}\right) \varphi_\mathcal{E}(-K\varphi_f c_{\text{enz}} + a_r \left(\varphi_f - \varphi_f^{\text{phys}}\right)). \end{aligned} \tag{14}$$

This equation expresses the conservation of the total mass of the tissue. A simple manipulation allows us to write (14) as

$$\begin{aligned} \varphi_s s_0 \left(\frac{\partial p}{\partial t} + \nabla p \cdot \mathbf{v}_s\right) + \nabla \cdot (\mathbf{v}_s + \varphi_f \mathbf{w}) &= Q_{\text{inj}}^{\text{tot}} + Q_{\text{vas}} - Q_{\text{lym}} \\ &+ \left(1 - \frac{\rho_s^{R,0}}{\rho_f^R}\right) \varphi_\mathcal{E}(-K\varphi_f c_{\text{enz}} + a_r \left(\varphi_f - \varphi_f^{\text{phys}}\right)). \end{aligned} \tag{15}$$

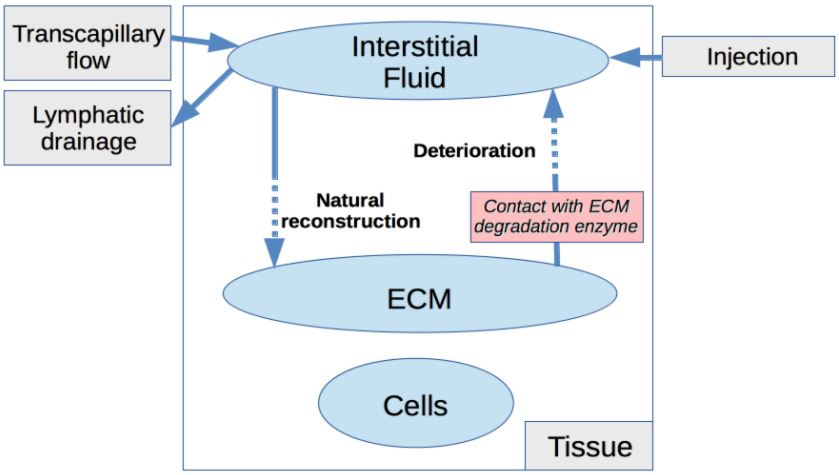

Fig. 6 Schematic description of exchange pathways and production terms of the different phases.

Remark 1 The term $\varphi_s s_0 \left(\frac{\partial p}{\partial t} + \nabla p \cdot \mathbf{v}_s\right)$ in Equation (15) comes from Assumptions 5 and 6. If the density in a homogeneous state of the solid phase were assumed to be a constant, this term would vanish.

2.2.3 Momentum balance for each component of the mixture

The momentum of the ζth constituent can change due to

1. the momentum flux caused by the motion at the velocity $\mathbf{v}_\zeta$ of the constituent,
2. contact forces within the constituent acting through the boundary,
3. contact forces due to the interaction with the other constituents within the domain through the interface separating the constituents,
4. momentum supply related to phase changes,
5. momentum supply related to external sources or sinks of mass.

One can then write the following local form of the momentum balance in conservative form

$$\frac{\partial}{\partial t}(\rho_\zeta \mathbf{v}_\zeta) + \boldsymbol{\nabla} \cdot (\rho_\zeta \mathbf{v}_\zeta \otimes \mathbf{v}_\zeta) = \boldsymbol{\nabla} \cdot \boldsymbol{\sigma}_\zeta + \boldsymbol{\pi}_\zeta + \rho_\zeta Q_\zeta \mathbf{v}_\zeta + \mathcal{S}_\zeta \mathbf{v}_\zeta,$$

where

- $\boldsymbol{\sigma}_\zeta$ is called the partial stress,
- $\boldsymbol{\pi}_\zeta$ is called the interaction force.

Actually using the mass balance equation (8), this equation can be simplified as

$$\rho_\zeta \left(\frac{\partial}{\partial t}\mathbf{v}_\zeta + \mathbf{v}_\zeta \cdot \boldsymbol{\nabla}\mathbf{v}_\zeta\right) = \boldsymbol{\nabla} \cdot \boldsymbol{\sigma}_\zeta + \boldsymbol{\pi}_\zeta, \tag{16}$$

where the inertial term on the left-hand side can usually be neglected when describing biological tissues (Barry and Aldis 1991; Barry and Mercer 1999). The reader may refer to (Giverso et al 2015) for a justification of this approximation. Let us recall that all the solid matrix constituents (cells and ECM) experience the same overall motion, so we can simplify the momentum balance equations for the tissue constituents into the a coupled system of PDEs to be solved in $\Omega_t \times (0, T)$:

$$\begin{cases} \boldsymbol{\nabla} \cdot \boldsymbol{\sigma}_f + \boldsymbol{\pi}_f = 0, & \text{(17a)} \\ \boldsymbol{\nabla} \cdot \boldsymbol{\sigma}_s + \boldsymbol{\pi}_s = 0, & \text{(17b)} \end{cases}$$

where (17b) is the equation resulting from the sum of (16) for $\zeta = \mathcal{E}, \not{c}$, and expresses the total momentum of the solid phase as a whole. In the case of a saturated mixture, it can be proved that (Bowen 1980)

$$\begin{cases} \boldsymbol{\sigma}_s = -\varphi_s p \mathbf{I} + \varphi_s \boldsymbol{\sigma}_s^E & \text{(18a)} \\ \boldsymbol{\sigma}_f = -\varphi_f p \mathbf{I} & \text{(18b)} \end{cases}$$

where $\boldsymbol{\sigma}_s^E$ is the effective stress tensor of the solid phase of the tissue, whose form will be discussed in Section 2.3, and where $p = p(t, \mathbf{x})$ is the pressure exerted by the fluid phase and $\mathbf{I}$ is the identity tensor. The isotropic stress $-p\mathbf{I}$ accounts for the coupling, typical of poroelasticity, between the fluid flow and the deformation of the solid matrix, and in particular describes the contribution to the stress due to the fluid pressure within the structure.
The quantities $\boldsymbol{\sigma}_\zeta$, for $\zeta \in \{s, f\}$, are the total stress tensors of the solid and fluid phases. As usual, we neglect the effective stress tensor of the fluid, meaning that we assume that the internal fluid viscosity is negligible compared with the friction between the fluid and the solid matrix (Barry and Mercer 1999). We observe that, for all $t \in (0, T)$ and at all $\mathbf{x} \in \Omega$, it holds (Preziosi and Tosin 2008)

$$\boldsymbol{\pi}_s(t, \mathbf{x}) + \boldsymbol{\pi}_f(t, \mathbf{x}) = 0. \tag{19}$$

2.2.4 Total momentum balance for the mixture

Summing equations (16) for $\zeta = s, f$ and using (18), we get

$$\boldsymbol{\nabla} \cdot (\varphi_s \boldsymbol{\sigma}_s^E) = \nabla p. \tag{20}$$

This equation expresses the conservation of total momentum of the tissue.

2.2.5 Mass balance for ECM degradation enzyme's concentration

Another fundamental quantity of interest from the modeling point of view is the concentration in ECM degradation enzyme, such as hyaluronidase or collagenase, per unit volume within the fluid phase of the tissue, $c_{\text{enz}} = c_{\text{enz}}(t, \mathbf{x})$. However, the concentration c_{enz} has to be related to the volume ratio occupied by the interstitial fluid. Finally the relevant entity for an overall balance over the whole tissue is the *reduced (or weighted) concentration*, e.g. $C_{\text{enz}} = \varphi_f c_{\text{enz}}$. The mass balance system (13) for the solid and fluid phases of the tissue is thus accompanied by a corresponding continuity equation for the hyaluronidase concentration that is transported throughout the tissue by the interstitial fluid. We consider that the reduced concentration can change due to

1. the motion of the fluid at the velocity $\mathbf{v}_f$,
2. the diffusive flux,
3. natural degradation and/or the intake due to the source.

Therefore, the following reaction-convection-diffusion equation reads

$$\frac{\partial}{\partial t}(\varphi_f c_{\text{enz}}) + \nabla \cdot (\varphi_f c_{\text{enz}} \mathbf{v}_f) = -\nabla \cdot (\varphi_f \mathbf{j}_{\text{enz}}^f) - k_{\text{enz}}^{d,\text{eff}} \varphi_f c_{\text{enz}} + \mathcal{S}_{\text{enz}}, \tag{21}$$

where

- $\mathbf{j}_{\text{enz}}^f$ is diffusive flux inside the liquid phase,
- $k_{\text{enz}}^{d,\text{eff}}$ is the net natural degradation effective rate of the enzyme in the interstitial fluid,
- $\mathcal{S}_{\text{enz}}$ is the contribution consecutive to the injection (directly into the tissue or intravenously) of enzyme.

Fick's law states that the diffusive flux can be assumed to be proportional to the concentration gradient in the liquid, that is

$$\mathbf{j}_{\text{enz}}^f = -\mathbf{D}_{\text{enz}}^f \nabla c_{\text{enz}}, \tag{22}$$

where $\mathbf{D}_{\text{enz}}^f$ is the effective diffusion tensor in the liquid, that we choose to be a tensor linearly dependent on the porosity (Magzoub et al 2008)

$$\mathbf{D}_{\text{enz}}^f = \varphi_f \mathbf{D}_{\text{enz}}^0. \tag{23}$$

Hence, equation (21) in terms of $C_{\text{enz}} = \varphi_f c_{\text{enz}}$ becomes

$$\frac{\partial C_{\text{enz}}}{\partial t} + \nabla \cdot (C_{\text{enz}} \mathbf{v}_f) = \nabla \cdot \left(\varphi_f^2 \mathbf{D}_{\text{enz}}^0 \nabla \left(\frac{C_{\text{enz}}}{\varphi_f} \right) \right) - k_{\text{enz}}^{d,\text{eff}} C_{\text{enz}} + \mathcal{S}_{\text{enz}}. \tag{24}$$

2.2.6 Mass balance for drug concentration

The main quantity of interest from the modeling point of view is the concentration in therapeutic agent per unit volume within the fluid phase of the tissue, $c_{\text{drug}} = c_{\text{drug}}(t, \mathbf{x})$. As previously, the concentration c_{drug} has to be related to the volume ratio the interstitial fluid. The relevant entity for an overall balance over the whole tissue is the *reduced (or weighted) concentration*, e.g. $C_{\text{drug}} = \varphi_f c_{\text{drug}}$. The continuity equation for the therapeutic agent's concentration that is transported throughout the tissue by the interstitial fluid can be deduced considering that the reduced concentration can change due to

1. the motion of the fluid
2. the diffusive flux
3. natural degradation and/or the intake due to the source.

Therefore, the following reaction-convection-diffusion equation can be deduced

$$\frac{\partial}{\partial t}(\varphi_f c_{\text{drug}}) + \nabla \cdot (\varphi_f c_{\text{drug}} \mathbf{v}_f) = -\nabla \cdot (\varphi_f \mathbf{j}^f_{\text{drug}}) - k^{d,\text{eff}}_{\text{drug}} \varphi_f c_{\text{drug}} + \mathcal{S}_{\text{drug}}, \tag{25}$$

where

- $\mathbf{j}^f_{\text{drug}}$ is diffusive flux inside the liquid phase,
- $k^{d,\text{eff}}_{\text{drug}}$ is the net natural degradation effective rate of the drug in the interstitial fluid,
- $\mathcal{S}_{\text{drug}}$ is the contribution consecutive to the injection (directly into the tissue or intravenously) of drug.

As before, Fick's law states that the diffusive flux can be assumed to be proportionnal to the concentration gradient in the liquid, that is

$$\mathbf{j}^f_{\text{drug}} = -\mathbf{D}^f_{\text{drug}} \nabla c_{\text{drug}}, \tag{26}$$

where $\mathbf{D}^f_{\text{drug}}$ is the effective diffusion coefficient in the liquid, that we choose to be linearly dependent on the porosity (Magzoub et al 2008)

$$\mathbf{D}^f_{\text{drug}} = \varphi_f \mathbf{D}^0_{\text{drug}}. \tag{27}$$

Hence, using (13c), equation (21) simplifies to

$$\frac{\partial C_{\text{drug}}}{\partial t} + \nabla \cdot (C_{\text{drug}} \mathbf{v}_f) = \nabla \cdot \left(\varphi_f^2 \mathbf{D}^0_{\text{drug}} \nabla \left(\frac{C_{\text{drug}}}{\varphi_f} \right) \right) - k^{d,\text{eff}}_{\text{drug}} C_{\text{drug}} + \mathcal{S}_{\text{drug}}. \tag{28}$$

2.3 Constitutive equations regarding the mechanical and fluid subsystems

2.3.1 Darcy's law

We assume the relative velocity to be expressed by Darcy's law (Ambrosi 2002; Basser 1992; Astanin and Preziosi 2008; Barry and Mercer 1999)

$$\varphi_f \mathbf{w} = \varphi(\mathbf{v}_f - \mathbf{v}_s) = -\boldsymbol{\kappa} \nabla p \tag{29}$$

where $\boldsymbol{\kappa}$ is the permeability tensor.

2.3.2 Starling's law

The transcapillary flow and the lymphatic drainage are taken into account in (12). Both rates Q_{vas} and Q_{lym} can be evaluated throught Starling's law. A complete description of the formulation of this law can be found in (Soltani and Chen 2012). The final result is

$$Q_{\text{vas}} - Q_{\text{lym}} = \frac{L_p S + L_{PL} S_L}{V} (p_v - p), \tag{30}$$

where L_p and L_{PL} are the hydraulic conductivities of the microvascular wall and of the lymphatic wall respectively; S/V and S_L/V are the surface area per unit volume of the vasculature and of the lymphatics respectively; and where p_v is the driving pressure. Equation (30) will be written as

$$Q_{\text{vas}} - Q_{\text{lym}} = \gamma(p_v - p), \tag{31}$$

where $\gamma = (L_p S + L_{PL} S_L)/V$ will be assumed to be a constant.

2.3.3 The linear elasticity framework

To complete our derivations of the equations of motion, we must know (or assume) the relationships (constitutive laws) between effective stress and strain. The classical theory of elasticity deals with the mechanical properties of elastic solids for which the stress is directly proportional to the stress in small deformations. Linear elastic theory can be satisfactorily applied for modeling the mechanical properties of biological media (Fung 1981; Mow et al 1984; Basser 1992; Bottaro and Ansaldi 2012): namely, we assume that biological tissues are nearly linear elastic under small strain and follow a constitutive law based on Hooke's law. Specifically, a Hookean elastic solid is a solid that obeys Hooke's Law, that states that the first Piola-Kirchhoff stress tensor $\mathbf{S}_s^E$ is such that

$$\mathbf{S}_{s;ij}^E = C_{ijkl}\boldsymbol{\varepsilon}_{kl} \tag{32}$$

where C_{ijkl} is the stiffness tensor and where $\boldsymbol{\varepsilon}$ is the infinitesimal strain (47) defined later in Section 3.

Remark 2 For most materials, the linear elasticity framework is only valid for small displacements (Rosler et al 2007).

Remark 3 In biomechanics, biological tissues are thought to be better described as viscoelastic solids (Fung 1981; Delingette 1998). However, for the sake of simplicity, we choose here to stay within the framework of the linear elasticity theory.

The first Piola-Kirchhoff stress tensor is then related to the Cauchy stress tensor (Batra 1998) via the deformation gradient $\mathbf{F}$ defined by (46) at Section 3

$$\boldsymbol{\sigma}_s^E = \frac{1}{J}\mathbf{F}\mathbf{S}_s^E\mathbf{F}^T. \tag{33}$$

Isotropic media. In the most simple symmetry case of an isotropic elastic solid, the material has only two independent elastic moduli, called the Lamé constants, λ and μ . In such a medium the elastic properties at any point are independent from direction. The Lamé constants are related to the stiffness tensor C_{ijkl} by

$$C_{ijkl} = \lambda\delta_{ij}\delta_{kl} + \mu\left(\delta_{ik}\delta_{jl} + \delta_{il}\delta_{jk}\right),$$

which gives us the following form for the effective stress $\mathbf{S}_s^E$

$$\mathbf{S}_s^E = 2\mu\boldsymbol{\varepsilon} + \lambda Tr(\boldsymbol{\varepsilon})\mathrm{I_d}. \tag{34}$$

As far as the diffusion tensors and the permeability tensor are concerned, in the isotropic case, we take

$$\mathbf{D}_{\text{enz}}^0 = D_{\text{enz}}^0\mathrm{I_d}, \qquad \mathbf{D}_{\text{drug}}^0 = D_{\text{drug}}^0\mathrm{I_d}, \qquad \boldsymbol{\kappa} = \kappa\mathrm{I_d}. \tag{35}$$

Transverse isotropic media. It is now well established that anisotropy plays a major role in the mechanical properties of biological media such as muscles, tendons or bones (Royer et al 2011). The simplest anisotropic model is the transverse isotropic one. A transversely isotropic tissue is characterized by the existence of a single plane of isotropy and one single axis of rotational symmetry, the normal to the isotropy plane. Skeletal muscle, for instance, consists of hundreds to thousands, sometimes millions, of long, multinucleated fibers organized and held together by an ECM thus it is relevant to model it as a transverse isotropic media.
In the case of a transverse isotropic medium in 2D, relation (32) reduces to (34) in the plane of isotropy (xy). If we consider the plane (xz), (32) can be written in the following way

$$\begin{pmatrix} \mathbf{S}_{s;11}^E \\ \mathbf{S}_{s;33}^E \\ \mathbf{S}_{s;13}^E \end{pmatrix} = \begin{pmatrix} C_{1111} & C_{1133} & 0 \\ C_{1133} & C_{3333} & 0 \\ 0 & 0 & C_{1313} \end{pmatrix} \begin{pmatrix} \varepsilon_{11} \\ \varepsilon_{33} \\ 2\varepsilon_{13} \end{pmatrix}. \tag{36}$$

It has been reported (Swartz and Fleury 2007) that the permeability $\boldsymbol{\kappa}$ depends on many factors including the geometry. Orientation can affect $\boldsymbol{\kappa}$, with perpendicular fibers providing a larger resistance to flow $\kappa_\perp$ than parallel fibers $\kappa_{/\!/}$. Consequently, in a rightful vector basis, we take $\boldsymbol{\kappa}$ as

$$\boldsymbol{\kappa} = \begin{pmatrix} \kappa_{/\!/} & 0 \\ 0 & \kappa_\perp \end{pmatrix}. \tag{37}$$

As far as the diffusion tensors are concerned, it was also reported (Cleveland et al 1976; Damon et al 2011) that the diffusion coefficient parallel to a skeletal muscle fiber's long axis $D^0_{\text{enz},/\!/}$ (resp. $D^0_{\text{drug},/\!/}$) is greater than the diffusion coefficient perpendicular to the fiber longest axis $D^0_{\text{enz},\perp}$ (resp. $D^0_{\text{drug},\perp}$). Consequently, in a rightful vector basis,

$$\mathbf{D}^0_{\text{enz}} = \begin{pmatrix} D^0_{\text{enz},/\!/} & 0 \\ 0 & D^0_{\text{enz},\perp} \end{pmatrix}, \qquad \text{resp. } \mathbf{D}^0_{\text{drug}} = \begin{pmatrix} D^0_{\text{drug},/\!/} & 0 \\ 0 & D^0_{\text{drug},\perp} \end{pmatrix}. \tag{38}$$

2.3.4 Degradation rates

The degree of porosity has a significant impact on the net natural degradation effective rate of the enzyme or the drug in the interstitial fluid $k^{d,\text{eff}}_{\text{enz}}, k^{d,\text{eff}}_{\text{drug}}$. The effects are both attributed to a wall effect and a surface area effect because the media with lower porosities or larger pores possess thicker pore walls and smaller surface area, which depress the diffusion of degradation products (Wu and Ding 2005). Consequently, we choose

$$k^{d,\text{eff}}_{\text{enz}} = \frac{k^d_{\text{enz}}}{\varphi_f} \text{ and } k^{d,\text{eff}}_{\text{drug}} = \frac{k^d_{\text{drug}}}{\varphi_f}, \tag{39}$$

where k^d_{enz} and k^d_{drug} are positive constants.

2.3.5 Source terms.

Let the index ω denote either of the chemical species of interest (enzyme and/or drug).

Injection. If the chemical species is directly injected in the tissue, we can choose to take the source term as

$$\mathcal{S}_\omega = c^\omega_{\text{inj}} Q^\omega_{\text{inj}}, \tag{40}$$

where c^ω_{inj} is the value of the species concentration injected, which is assumed to be a constant. In the numerical simulations of sections 4 and 5, Q^ω_{inj} is a Gaussian function with a very small spread

$$Q^\omega_{\text{inj}} = q^\omega_{\text{inj}} \exp\left(-\sum_{i=1}^{d} \frac{(x_i - x^0_i)^2}{2\sigma^2_{x_i}} \right), \tag{41}$$

where $q^\omega_{\text{inj}}, \sigma_{x_i}$ are positive constants and where $(x^0_1, \ldots, x^0_d)$ indicate the coordinates of the injection point.

Incubation. If the tissue is incubated in the chemical species, the source term $\mathcal{S}_\omega$ is taken as zero and and we choose instead to apply a non homogeneous Dirichlet boundary condition on C_ω (cf section 5).

Transcapillary transport. If the chemical species are injected intravenously, we choose to take the source term accordingly with the pore model for transcapillary exchange via convection stated in (Baxter and Jain 1989)

$$\mathcal{S}_\omega = (1 - \gamma_c)(Q_{\text{vas}} - Q_{\text{lym}}) c^\omega_v, \tag{42}$$

where γ_c represents the coupling between fluid and solute and c^ω_v is the plasma concentration of the chemical species. In the numerical simulations of section 5, for the sake of simplicity,

$$c^\omega_v = c^\omega_{v,0}\, \chi_{|t_1 \le t \le t_2}, \tag{43}$$

where $c^\omega_{v,0}$ is a constant, and $[t_1, t_2]$ is the time interval of presence in the capillary network. c^ω_v can be chosen to follow any pharmacokinetic model of interest.

3 Formulation of the poroelastic model in the Lagrangian domain

3.1 Kinematics of the mixture

The motion of the constituents is described by the position occupied at time t by the particle labelled $\mathbf{X}$

$$\mathbf{x} = \Phi(t, \mathbf{X}), \tag{44}$$

$\mathbf{X}$ being the position of the particle in the reference configuration Ω_0. The function $\Phi(t, .)$ represents a mapping from initial (undeformed) configuration Ω_0 to the present (deformed) configuration Ω_t.

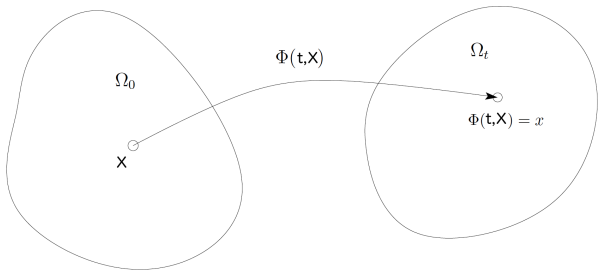

Fig. 7 Deformation from the fixed domain Ω_0 via the application Φ

The velocity of a particle belonging to the ζth constituent, often termed the Lagrangian velocity, $\mathbf{V}_\zeta(t, \mathbf{X})$, is the time rate change of the particle position holding $\mathbf{X}$ fixed. As we will use the Eulerian formalism to state conservation equations, we recall that the Eulerian velocity at time t and position $\mathbf{x}$, $\mathbf{v}_\zeta(t, \mathbf{x})$, is given by

$$\mathbf{v}_\zeta\left(t, \Phi(t, \mathbf{X})\right) = \mathbf{V}_\zeta(t, \mathbf{X}). \tag{45}$$

The configuration gradient, or deformation gradient, is defined by

$$\mathbf{F} := \frac{\partial \mathbf{x}}{\partial \mathbf{X}} = \left(\frac{\partial x_i}{\partial X_j}\right)_{i,j=1..d} \tag{46}$$

We also set $J := \det(\mathbf{F})$. We stated that all the solid matrix constituents (cells and ECM) experience the same overall motion (Sacco et al 2017). The displacement vector of the solid phase will be denoted $\mathbf{u} = \mathbf{u}(t, \mathbf{X})$. Note that we then have

$$\mathbf{V}_s(t, \mathbf{X}) = \frac{\partial}{\partial t}\mathbf{u}(t, \mathbf{X}).$$

We also define the associated infinitesimal deformation of the volume surrounding the point $\mathbf{X}$ at time t as

$$\varepsilon(t, \mathbf{X}) = \frac{1}{2}\left(\nabla\mathbf{u}(t, \mathbf{X}) + (\nabla\mathbf{u}(t, \mathbf{X})^T\right). \tag{47}$$

It is also useful to define the material time derivative following the solid matrix

$$\frac{D(\cdot)}{Dt} = \frac{\partial(\cdot)}{\partial t} + (\mathbf{v}_s \cdot \nabla)(\cdot) \quad . \tag{48}$$

3.2 Change of variables

From now on, the medium is assumed to be isotropic. The formulation in a transverse isotropic medium will be similar as only equation (54b) will change. To reduce the governing equations to the reference fixed domain Ω_0, we introduce a suitable change of variable, which is given by the motion function (44): $\mathbf{x} = \Phi(t, \mathbf{X})$.

If $\mathbf{u}(t,\mathbf{X}) = \mathbf{x} - \mathbf{X}$ is the displacement vector, Φ is given by

$$\Phi(t,\mathbf{X}) = \mathbf{X} + \mathbf{u}(t,\mathbf{X}). \tag{49}$$

Let us set

$$\begin{aligned}
&f(t,\mathbf{X}) := \varphi_f(t,\Phi(t,\mathbf{X})),\ f^{\text{phys}}(t,\mathbf{X}) := \varphi_f^{\text{phys}}(\Phi(t,\mathbf{X})),\\
&g_{\mathcal{E}}(t,\mathbf{X}) := \varphi_{\mathcal{E}}(t,\Phi(t,\mathbf{X})),\ g_{\mathcal{C}}(t,\mathbf{X}) := \varphi_{\mathcal{C}}(t,\Phi(t,\mathbf{X})),\ g_s(t,\mathbf{X}) := \varphi_s(t,\Phi(t,\mathbf{X})),\\
&P(t,\mathbf{X}) := p(t,\Phi(t,\mathbf{X})),\ P_v(t,\mathbf{X}) := p_v(t,\Phi(t,\mathbf{X})),\\
&h(t,\mathbf{X}) := C_{\text{enz}}(t,\Phi(t,\mathbf{X})),\ c(t,\mathbf{X}) := C_{\text{drug}}(t,\Phi(t,\mathbf{X})),
\end{aligned}$$

Recall that we have already from Section 2.3

$$\mathbf{v}_s(t,\Phi(t,\mathbf{X})) = \mathbf{V}_s(t,\mathbf{X}) = \frac{\partial}{\partial t}\mathbf{u}(t,\mathbf{X}), \tag{50}$$

and

$$\boldsymbol{\sigma}_s^E = \frac{1}{J}\mathbf{F}\,\mathbf{S}_s^E\,\mathbf{F}^T \text{ with } \mathbf{S}_s^E = 2\mu\boldsymbol{\varepsilon} + \lambda Tr(\boldsymbol{\varepsilon})\mathrm{I_d}, \tag{51}$$

since we consider the isotropic case. Moreover, every time and space derivative are affected by the change of variables in the following way (example on $f = \varphi_f$):

$$\frac{D\varphi_f}{Dt} = \frac{\partial f}{\partial t},\quad \nabla_{\mathbf{x}}\,\varphi_f = \mathbf{F}^{-1}\,\nabla_{\mathbf{X}}\,f. \tag{52}$$

3.3 Non-dimensionalization

We state that from now ∇ denotes the operator $\nabla_{\mathbf{X}} = (\partial_{X_1},\dots,\partial_{X_d})^T$. Denote by l_0 the typical length of the porous medium. We non-dimensionalize the governing equations by letting

$$\begin{aligned}
&\mathbf{X} = l_0\overline{\mathbf{X}}, \qquad \mathbf{u} = l_0\overline{\mathbf{u}}, \quad t = \frac{l_0^2}{\kappa(\lambda+2\mu)}\overline{t}, \quad \mathbf{V}_s = \frac{\kappa(\lambda+2\mu)}{l_0}\overline{\mathbf{V}_s},\\
&P = (\lambda+2\mu)\overline{P}, \quad h = c_0\overline{h}, \quad c = c_0\overline{c},
\end{aligned}$$

where we use bars to denote the dimensionless variables. The dimensionless Piola-Kirchhoff and Cauchy stress tensors are defined as $\overline{\mathbf{S}_s^E} = \mathbf{S}_s^E/(\lambda+2\mu)$ and $\overline{\boldsymbol{\sigma}_s^E} = \boldsymbol{\sigma}_s^E/(\lambda+2\mu)$, respectively, and we define the dimensionless parameters

$$\begin{aligned}
&\overline{\mu} = \frac{\mu}{\lambda+2\mu}, && \overline{\lambda} = \frac{\lambda}{\lambda+2\mu}, && \overline{s_0} = s_0(\lambda+2\mu), && \overline{\boldsymbol{\kappa}} = \frac{1}{\kappa}\boldsymbol{\kappa},\\
&\alpha = \frac{l_0^2}{\kappa(\lambda+2\mu)}, && \overline{K} = \alpha c_0 K, && \overline{a_r} = \alpha a_r, && \overline{\gamma} = \frac{l_0^2}{\kappa}\gamma,\\
&\overline{\mathbf{D}_{\text{enz}}^0} = \frac{1}{\kappa(\lambda+2\mu)}\mathbf{D}_{\text{enz}}^0, && \overline{k_{\text{enz}}^d} = \alpha k_{\text{enz}}^d, && \overline{P_v} = \frac{P_v}{\lambda+2\mu},\\
&\overline{\mathbf{D}_{\text{drug}}^0} = \frac{1}{\kappa(\lambda+2\mu)}\mathbf{D}_{\text{drug}}^0, && \overline{k_{\text{drug}}^d} = \alpha k_{\text{drug}}^d.
\end{aligned}$$

We choose the $(\lambda+2\mu)$ parameter as a natural pressure scale; by this choice the dimensionless elastic parameters $\overline{\lambda},\overline{\mu}$ are of order 1 (Lang et al 2016).

3.4 Simplification of the model

The governing equations in Ω_t can be reformulated on the fixed reference domain Ω_0 dimensionless. The first advantage of this process is to obtain a system of equations in a fixed reference domain in order to make the numerical processing possible. Second, the constitutive relation on the stress tensor $\mathbf{S}_s^E$ is given in the lagrangian coordinates $(t, \mathbf{X})$, so it is natural to work within this system of coordinates. The third benefit is to elude the transport equations of the three different volume fractions: in the fixed reference domain, those equations reduce to ordinary differential equations.
The calculus in the general case is presented in Appendix A. For the sake of simplicity, we assume that our system undergoes very small perturbations (see Remark 2), meaning that

$$\mathbf{F}^{-1} = \mathrm{I_d} + \mathcal{M}(\nabla \mathbf{u}),$$

where the matrix $\mathcal{M}(\nabla \mathbf{u})$ is negligible. Thus we can write the system with $\mathbf{F}^{-1} = \mathbf{F} = \mathrm{I_d}$. Let us set

$$J_{\text{enz}} = \frac{1}{f}\overline{\boldsymbol{\kappa}}\,\nabla P - \overline{\mathbf{D}^0_{\text{enz}}}\nabla f \qquad \text{and} \qquad J_{\text{drug}} = \frac{1}{f}\overline{\boldsymbol{\kappa}}\,\nabla P - \overline{\mathbf{D}^0_{\text{drug}}}\nabla f. \tag{53}$$

The equivalent system in Ω_0 in dimensionless form in this simplified case reads

$$\begin{cases}
g_{\mathcal{E}} + g_{\mathcal{C}} + f = 1, & \text{(54a)}\\
\boldsymbol{\nabla}\cdot\left((g_{\mathcal{E}} + g_{\mathcal{C}})\left(\overline{\lambda}(\nabla\cdot\mathbf{u})I + \overline{\mu}(\nabla\mathbf{u} + \nabla\mathbf{u}^T)\right)\right) = \nabla P, & \text{(54b)}\\
(g_{\mathcal{E}} + g_{\mathcal{C}})\overline{s_0}\dfrac{\partial P}{\partial t} - \nabla\cdot(\overline{\boldsymbol{\kappa}}\,\nabla P) = \alpha\, Q^{\text{tot}}_{\text{inj}} + \overline{\gamma}(\overline{P_v} - P) & \\
\qquad + \left(\dfrac{\rho_s^{R,0}}{\rho_f^R} - 1\right) g_{\mathcal{E}}(\overline{K}h + \overline{a_r}(f^{\text{phys}} - f)) - \nabla\cdot\left(\dfrac{\partial \mathbf{u}}{\partial t}\right), & \text{(54c)}\\
\dfrac{\partial h}{\partial t} = \nabla\cdot(f\overline{\mathbf{D}^0_{\text{enz}}}\nabla h + hJ_{\text{enz}}) + h\left(-\dfrac{\overline{k^d_{\text{enz}}}}{f} - \nabla\cdot\left(\dfrac{\partial \mathbf{u}}{\partial t}\right)\right) + \dfrac{\alpha\mathcal{S}_{\text{enz}}}{c_0}, & \text{(54d)}\\
\dfrac{\partial g_{\mathcal{C}}}{\partial t} + \left(\overline{s_0}\dfrac{\partial P}{\partial t} + \nabla\cdot\left(\dfrac{\partial \mathbf{u}}{\partial t}\right)\right) g_{\mathcal{C}} = 0, & \text{(54e)}\\
\dfrac{\partial g_{\mathcal{E}}}{\partial t} + \left(\overline{K}h + \overline{a_r}(f^{\text{phys}} - f) + \overline{s_0}\dfrac{\partial P}{\partial t} + \nabla\cdot\left(\dfrac{\partial \mathbf{u}}{\partial t}\right)\right) g_{\mathcal{E}} = 0, & \text{(54f)}\\
\dfrac{\partial c}{\partial t} = \nabla\cdot(f\overline{\mathbf{D}^0_{\text{drug}}}\nabla c + cJ_{\text{drug}}) + c\left(-\dfrac{\overline{k^d_{\text{drug}}}}{f} - \nabla\cdot\left(\dfrac{\partial \mathbf{u}}{\partial t}\right)\right) + \dfrac{\alpha\mathcal{S}_{\text{drug}}}{c_0}. & \text{(54g)}
\end{cases}$$

Remark 4 ***(Influence of the solid phase deformation)*** The influence of the solid phase deformation $\mathbf{u}$ on the diffusion of the enzyme h and on the transcapillary transport of the drug c appears in 3 terms. The first direct influence occurs through the time derivative of $\nabla\cdot u$, which is negligible. In addition, the deformation impacts also the fluid phase f and the terms J_{enz} and J_{drug}, which affect the diffusion of both h and c. Indeed, the solid phase deformation $\mathbf{u}$ is linked to the pressure P. Therefore, even if the solid deformation is small and does not appear straightforwardly in the transport of h and c, it has a non negligible influence.

Remark 5 ***(Dynamics added on the porosity)*** In previous studies, the porosity of the medium (or volume fraction of fluid) is often regarded as a constant (Basser 1992). Models that include porosity changes (Netti et al 1997) have used the following relation between $\nabla\cdot\mathbf{u}$ and φ_f:

$$f = \frac{f^{\text{phys}} + \nabla\cdot\mathbf{u}}{1 + \nabla\cdot\mathbf{u}},$$

which is obtained traducing an hypothesis of infinitesimal displacement on the variation of volume, or more recently (Støverud et al 2011)

$$f = 1 - (1 - f^{\text{phys}})e^{-\nabla\cdot\mathbf{u}},$$

which is obtained from Equation (54e) in the case of a biphasic system with only incompressible cells and incompressible fluid. However, in our case, since our main hypothesis is that the porosity is not only affected by the deformation of the medium but mostly by the ECM degradation enzyme injected, we must derive an expression for the effective porosity directly from the mass balance laws of the ECM and cells constituents.
An expression for the effective volume fraction occupied by cells can be derived from the volume balance of the phase occupied by cells assuming the initial conditions $g_{\mathscr{C}}(0,\mathbf{x}) = g^0_{\mathscr{C}}(\mathbf{x})$ and $\nabla \cdot \mathbf{u}(0,\mathbf{x}) = 0$. Integrating Equation (54e),

$$g_{\mathscr{C}}(t,\mathbf{x}) = g^0_{\mathscr{C}}(\mathbf{x}) e^{-\nabla\cdot\mathbf{u} - \overline{s_0}(P-P^0)}. \tag{55}$$

To obtain the effective volume fraction occupied by ECM, consider

$$\tilde{g}_{\mathcal{E}} = g_{\mathcal{E}} e^{\nabla\cdot\mathbf{u} + \overline{s_0}(P-P^0)}. \tag{56}$$

An equation for this quantity assuming the initial conditions $\nabla \cdot \mathbf{u}(0,\mathbf{x}) = 0$, $P(0,\mathbf{x}) = P^0(\mathbf{x})$ and $\tilde{g}_{\mathcal{E}}(0,\mathbf{x}) = g_{\mathcal{E}}(0,\mathbf{x}) = g^0_{\mathcal{E}}(\mathbf{x})$, is given by

$$\frac{\partial \tilde{g}_{\mathcal{E}}}{\partial t} + \left(\overline{K}h + \overline{a_r}(f^{\text{phys}} - f)\right)\tilde{g}_{\mathcal{E}} = 0.$$

This equation reflects the fact that, regardless of the mechanical changes due to the displacement and the compressibility of the tissue, the ECM is deteriorated when in contact with the ECM degradation enzyme. The self-reconstruction of ECM towards the physiological state occurs at the rate $\overline{a_r}$.

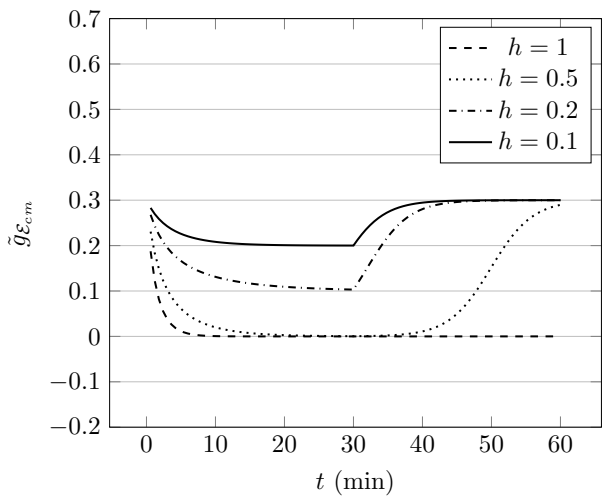

Fig. 8 $\tilde{g}_{\mathcal{E}}$ is plotted versus time for an initial volume fraction of ECM of 0.3 and for different concentrations of enzyme applied continuously during 30 minutes, regardless of the space dependency. Both tendencies (degradation during injection - reconstruction) can easily be observed.

3.5 Boundary conditions

The primary variables of the problem are the displacement $\mathbf{u}$, the pressure P and the concentrations in ECM degradation enzyme h and in therapeutic agent c. Define the boundary of the domain Ω, denoted Γ. We generically denote by $\mathbf{n}$ the normal to Ω outwardly directed from the inside to the outside of the domain. Next, define the portions of the boundary Γ_u and Γ_t on which displacement and stress are defined, such as $\Gamma_u \cup \Gamma_t = \Gamma$ and

$$\mathbf{u} = \mathbf{u}_{\Gamma_u} \text{ on } \Gamma_u \text{ and } \mathbf{S}^E_s\,\mathbf{n} = \mathbf{t} \text{ on } \Gamma_t. \tag{57}$$

Applying the condition $\mathbf{S}^E_s\,\mathbf{n} = 0$ to the boundary amounts to considering a free boundary, while setting $\mathbf{u}_{\Gamma_u} = 0$ amounts to considering a fixed boundary.
The portions of the boundary Γ_p and Γ_q are the parts of the boundary on which pressure and pressure flux are specified, such as $\Gamma_p \cup \Gamma_q = \Gamma$ and

$$P = P_{\Gamma_p} \text{ on } \Gamma_p \text{ and } \nabla P \cdot \mathbf{n} = q \text{ on } \Gamma_q. \tag{58}$$

Setting a Dirichlet condition on the pressure amounts to considering a permeable boundary in contact with a surrounding medium where the pressure is fixed, while applying the condition $\nabla P \cdot \mathbf{n} = 0$ amounts to considering a wall boundary condition.
The portions of the boundary Γ_h and Γ_β are the parts of the boundary on which the enzyme's concentration and flux are specified, such as $\Gamma_h \cup \Gamma_\beta = \Gamma$ and

$$\begin{cases} h = h_{\Gamma_h} \text{ on } \Gamma_h, & (59a) \\ \left(f\mathbf{D}^0_{\text{enz}} \nabla h + hJ_{\text{enz}}\right) \cdot \mathbf{n} = \beta_1 \text{ on } \Gamma_\beta. & (59b) \end{cases}$$

The same type of boundary conditions are applied to the therapeutic agent's concentration and flux

$$\begin{cases} c = c_{\Gamma_h} \text{ on } \Gamma_h, & (60a) \\ \left(f\mathbf{D}^0_{\text{drug}} \nabla c + cJ_{\text{drug}}\right) \cdot \mathbf{n} = \beta_2 \text{ on } \Gamma_\beta. & (60b) \end{cases}$$

4 Numerical simulations

4.1 Computational algorithm

We first need to reduce the whole coupled system (54) to a sequence of linearized equations of simpler form. We subdivide the time interval $[0, T]$ into $N \geq 1$ uniform subintervals of length $\Delta t = \frac{T}{N}$, in such a way that the discrete time levels $t^n = n\Delta t$, $n = 0, \ldots, N$, are obtained. We set

$$\nabla \cdot \mathbf{u}^0 = 0, \quad g^0_{\mathcal{E}} = g_{\mathcal{E}}(0, \mathbf{x}), \quad \tilde{g}^0_{\mathcal{E}} = g_{\mathcal{E}}(0, \mathbf{x}), \quad g^0_{\mathcal{C}} = g_{\mathcal{C}}(0, \mathbf{x}), \quad h^0 = 0 \text{ and } c^0 = 0, \tag{61}$$

and P^0 is set as the solution of the steady-state pressure equation:

$$-\nabla \cdot (\overline{\boldsymbol{\kappa}} \nabla P^0) = \overline{\gamma}(\overline{p_v} - P^0), \tag{62}$$

coupled with the boundary conditions (58).
For $n = 0, \ldots, N-1$, we perform the following iteration:

1. We obtain f^n using (54a): $f^n = 1 - g^n_{\mathcal{E}} - g^n_{\mathcal{C}}$, and we set $g^n_s = g^n_{\mathcal{E}} + g^n_{\mathcal{C}}$.
2. We obtain $\mathbf{u}^{n+1}$ and P^{n+1} solving the linear poroelastic system with the finite element solver FreeFem++ (Hecht 2012), choosing P_2 (resp. P_1) elements for $\mathbf{u}^{n+1}$ (resp. P^{n+1}) to guarantee stable Galerkin approximation (Feng et al 2014; Murad and Loula 1992) and discretizing in time with a first order backward Euler scheme (Murad and Loula 1994). Note that having a parabolic equation on P, which is a consequence of Assumption 3, numerically permits to prevent element locking (Phillips and Wheeler 2009).

$$\begin{cases} \nabla \cdot \left(g^n_s \left(\overline{\lambda}(\nabla \cdot \mathbf{u}^{n+1})I + 2\overline{\mu}\boldsymbol{\varepsilon}(\mathbf{u}^{n+1})\right)\right) - \nabla P^{n+1} = 0, & (63a) \\ g^n_s \overline{s_0} \dfrac{P^{n+1}}{\Delta t} - \nabla \cdot (\overline{\boldsymbol{\kappa}} \nabla P^{n+1}) + \overline{\gamma} P^{n+1} + \dfrac{\nabla \cdot \mathbf{u}^{n+1}}{\Delta t} = g^n_s \overline{s_0} \dfrac{P^n}{\Delta t} + \dfrac{\nabla \cdot \mathbf{u}^n}{\Delta t} & \\ \qquad + \alpha\, Q^{\text{tot}}_{\text{inj}}(t^{n+1}) + \overline{\gamma}\, \overline{p_{eq}} + \left(\dfrac{\rho^{R,0}_s}{\rho^R_f} - 1\right) g^n_{\mathcal{E}} (\overline{K} h^n + \overline{a_r}(f^{\text{phys}} - f^n)), & (63b) \end{cases}$$

supplied by the approximation of the boundary conditions (57) and (58)

$$\begin{cases} \mathbf{u}^{n+1} = \mathbf{u}_{\Gamma_u} \text{ on } \Gamma_u \text{ and } \mathbf{S}^{E,n+1}_s \mathbf{n} = \mathbf{t} \text{ on } \Gamma_t, & (64a) \\ P^{n+1} = P_{\Gamma_p} \text{ on } \Gamma_p \text{ and } \nabla P^{n+1} \cdot \mathbf{n} = q \text{ on } \Gamma_q. & (64b) \end{cases}$$

3. Let us denote

$$J^n_{\text{enz}} = \frac{1}{f^n}\overline{\boldsymbol{\kappa}}\nabla P^n - \overline{\mathbf{D}^0_{\text{enz}}}\nabla f^n \qquad \text{and} \qquad J^n_{\text{drug}} = \frac{1}{f^n}\overline{\boldsymbol{\kappa}}\nabla P^n - \overline{\mathbf{D}^0_{\text{drug}}}\nabla f^n. \tag{65}$$

We obtain h^{n+1} and c^{n+1} solving the linear advection-diffusion-reaction equations still using the finite element solver FreeFem++ (Hecht 2012)

$$\frac{h^{n+1}}{\Delta t} - \nabla\cdot(f^n\overline{\mathbf{D}^0_{\text{enz}}}\nabla h^{n+1} + h^{n+1}J^n_{\text{enz}}) - h^{n+1}\left(-\frac{\overline{k^d_{\text{enz}}}}{f^n} - \left(\frac{\nabla\cdot\mathbf{u}^{n+1} - \nabla\cdot\mathbf{u}^n}{\Delta t}\right)\right) = \frac{h^n}{\Delta t} + \frac{\alpha}{c_0}\mathcal{S}_{\text{enz}}(t^{n+1}), \tag{66}$$

and

$$\frac{c^{n+1}}{\Delta t} - \nabla\cdot(f^n\overline{\mathbf{D}^0_{\text{drug}}}\nabla c^{n+1} + c^{n+1}J^n_{\text{drug}}) - c^{n+1}\left(-\frac{\overline{k^d_{\text{drug}}}}{f^n} - \left(\frac{\nabla\cdot\mathbf{u}^{n+1} - \nabla\cdot\mathbf{u}^n}{\Delta t}\right)\right) = \frac{c^n}{\Delta t} + \frac{\alpha}{c_0}\mathcal{S}_{\text{drug}}(t^{n+1}), \tag{67}$$

supplied by the following approximation of the boundary conditions (59) and (60):

$$\begin{cases} h^{n+1} = h_{\Gamma_h} \text{ on } \Gamma_h, \text{ and } \left(f^n\mathbf{D}^0_{\text{enz}}\nabla h^{n+1} + h^{n+1}J^n_{\text{enz}}\right)\cdot\mathbf{n} = \beta_1 \text{ on } \Gamma_\beta, & \text{(68a)} \\ c^{n+1} = h_{\Gamma_h} \text{ on } \Gamma_h, \text{ and } \left(f^n\mathbf{D}^0_{\text{drug}}\nabla c^{n+1} + c^{n+1}J^n_{\text{drug}}\right)\cdot\mathbf{n} = \beta_2 \text{ on } \Gamma_\beta. & \text{(68b)} \end{cases}$$

4. We obtain $g^{n+1}_{\mathcal{E}}$ by first calculating

$$\tilde{g}^{n+1}_{\mathcal{E}} = \frac{\tilde{g}^n_{\mathcal{E}}}{1 + \Delta t(\overline{K}h^{n+1} + \overline{a_r}(f^{\text{phys}} - f^n))}.$$

and from (56), we deduce

$$g^{n+1}_{\mathcal{E}} = \tilde{g}^{n+1}_{\mathcal{E}} e^{-\nabla\cdot\mathbf{u}^{n+1} - \overline{s_0}(P^{n+1} - P^0)}.$$

To obtain $g^{n+1}_{\mathcal{C}}$, we use formula (55)

$$g^{n+1}_{\mathcal{C}} = g^0_{\mathcal{C}}(\mathbf{x}) e^{-\nabla\cdot\mathbf{u}^{n+1} - \overline{s_0}(P^{n+1} - P^0)}.$$

*Remark 6 (**Triangulation convergence tests**)* We checked numerically that the relative error e_h (resp. e_f, e_P) on the total mass of enzyme (resp. the quantity of fluid, the mean pressure) at $t = 60$ min decreases with order 1 when refining the mesh (Figure 9).

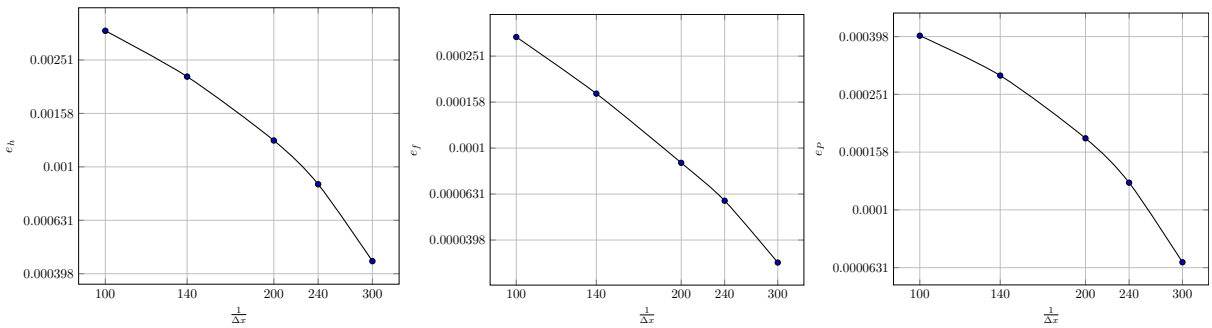

Fig. 9 Results from the triangulation convergence simulations in 1D at $t = 60$ min (simulations from section 4.2). The relative error on $\int_\Omega Z(t = 60 \text{ min})\,dx$ with $Z = h, f, P$ is plotted using logarithmic scales on both the horizontal and vertical axes.

*Remark 7 (**Mass conservation**)* A test case is performed to check if the total mass of enzyme injected is conserved when its degradation rate is zero. When the degradation rate is nonzero, the enzyme's total mass remains positive, and after reaching a maximum amount at the end of the injection, it decreases gradually till reaching zero as it has been observed in (Namazi et al 2016) (Figure 10).

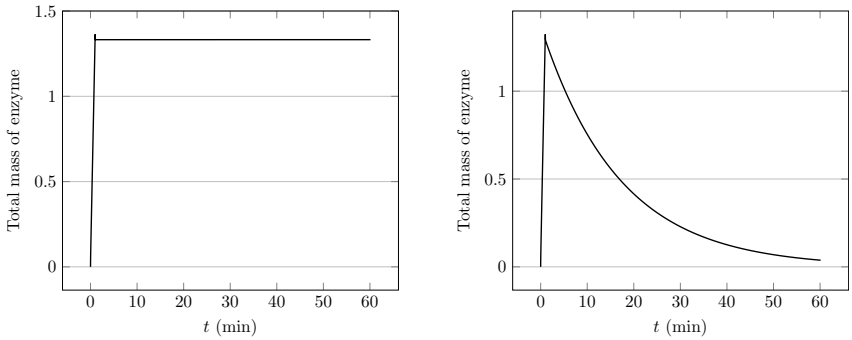

(a) Numerical mass conservation of enzyme.

(b) ECM degradation enzyme's total mass versus time when degradation rate is nonzero.

Fig. 10 First numerical results on the total mass of enzyme. Numerically, the mass is well conserved when the degradation rate is zero, while the curve has the expected shape when the degradation rate is nonzero.

4.2 Numerical tests in 1D

The computational domain. In this section, we formulate the poroelastic transport model in a one-dimensional geometrical configuration (1D). Figure 11 shows a schematic representation of the 1D reference domain we considered. Denoting by x the spatial coordinate, the region $x < 0$ represents the tissue far away from the site of injection, the open interval $\Omega = (0, L)$ is the tissue whereas the region $x > L$ corresponds to the air surrounding the tissue.

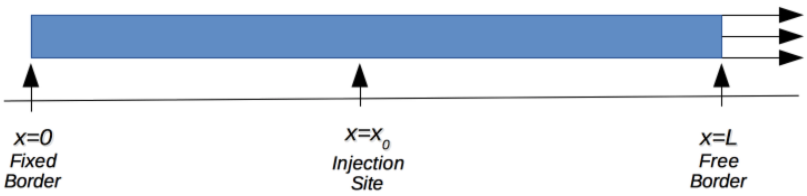

Fig. 11 Schematic representation of the 1D reference domain.

Simulation Tests. What we want here is to understand the qualitative effect on the porosity of a injection of ECM degradation enzyme. Consequently, we consider in this section system (54) without equation (54g). In the simulations, $\overline{\gamma}$ is chosen so the initial pressure, derived from equation (62), is a constant.
To test the capability of the model, simulations are performed on the homogeneous domain represented in Figure 11. The border of the domain is divided in two parts: $\Gamma = \Gamma_0 \cup \Gamma_f$. On Γ_0 $(x = 0)$, Dirichlet boundary conditions are imposed, i.e. displacement $\mathbf{u}$ and concentration h are set to zero, and pressure P is set to $\overline{p_v}$. On Γ_f $(x = 1)$, a free boundary condition is imposed on the displacement, i.e. $\mathbf{S}_s^E \mathbf{n} = 0$, while a wall condition is imposed on the pressure and the concentration h, i.e. $\nabla P \cdot \mathbf{n} = 0$ and $\left(\mathbf{D}^0_{\text{enz}} \nabla h + h J_{\text{enz}}\right) \cdot \mathbf{n} = 0$. Visualization with the software FreeFem++ allows us to plot the porosity f and any other quantities of interest directly in a changing domain thanks to the function movemesh (Hecht 2012).
The principal scope of these numerical experiments is to understand the qualitative behavior of the porosity after an injection of ECM degradation enzyme. Four sets of simulation tests are performed to investigate respectively the transport and effect of a passive substance (like water), the sole effect of degradation of the ECM by the enzyme injected, the effect of the enzyme on the ECM with recovery and the effect of the enzyme on the ECM with natural degradation of the enzyme. The fifth set of simulations corresponds to investigating how all the different effects interact together. Table 1 sums up these five different sets of simulations.

Table 1 Investigation of the effects on porosity of the parameters for each simulation test.

	K	a_r	k^d_{enz}	Considered Phenomena
Simulation 1	0	0	0	Passive transport
Simulation 2	0.5	0	0	Effect on ECM
Simulation 3	0.5	0.01	0	Effect on ECM + Recovery
Simulation 4	0.5	0	0.001	Effect on ECM + Natural degradation
Simulation 5	0.5	0.01	0.001	Effect on ECM + Recovery + Natural degradation

Simulations are performed first on the computational domain described in Figure 11 and the effects on the porosity f are investigated. Figures 12 represent the porosity of the medium at four different times for each simulation: after 1 minute, 10 minutes, 30 minutes and 1 hour.

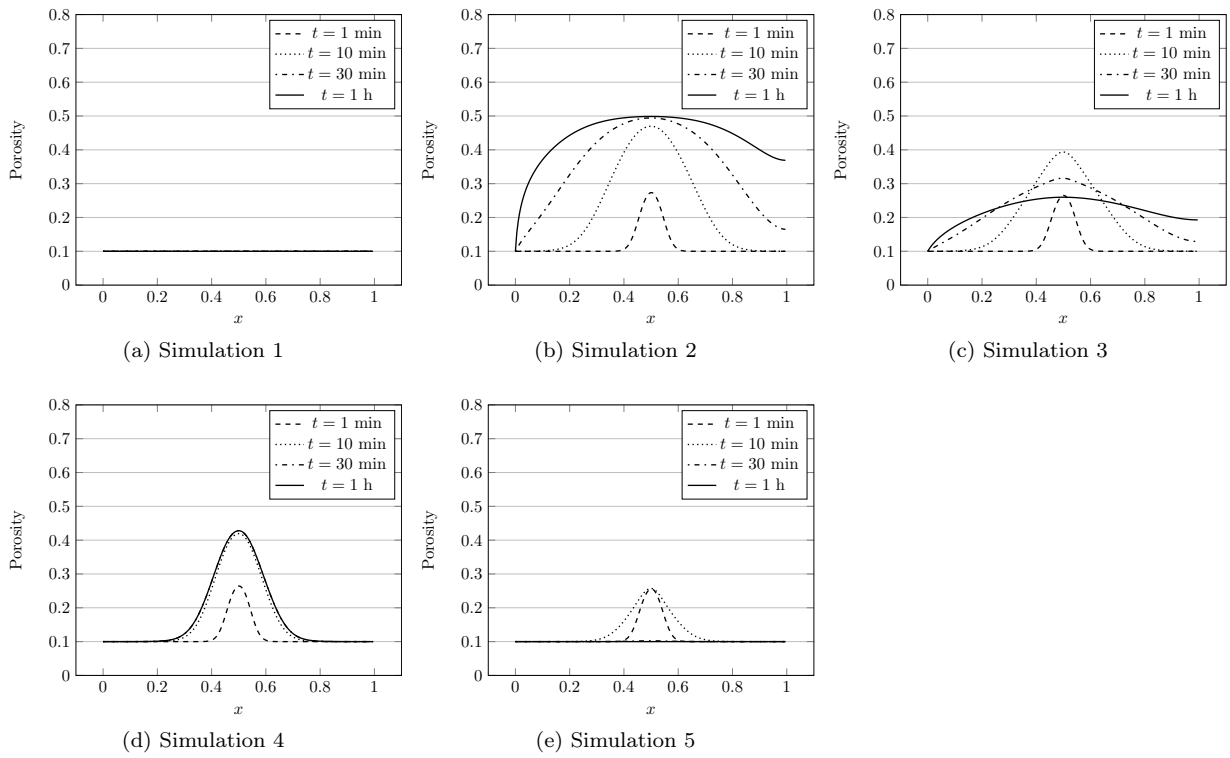

(a) Simulation 1 (b) Simulation 2 (c) Simulation 3

(d) Simulation 4 (e) Simulation 5

Fig. 12 Porosity changes at $t = 1$ min, 10 min, 30 min and 1 hour in the 1D case.

In the case of passive transport of water, the porosity remains equal to its initial value (0.1 in all four simulations). In reality, the porosity varies a little bit because of the volume variation, but when plotted between 0 and 1 it is not obvious and it seems legitimate to assume that the porosity is a constant in this case (12a). In the second set of simulations, we want to investigate the sole effect of degradation of the ECM by the enzyme, without recovery of the tissue and without natural degradation of the enzyme. With $K = 0.01$, the effect of the enzyme on the ECM is immediate: after 1 minute, the ECM around the injection site has been deteriorated. Then, with the diffusion of the enzyme, the area of degraged ECM expands mostly towards the boundary Γ_f as the enzyme flows out the domain through boundary Γ_0, without ever overcrossing the maximum value possible $f + g_{\mathcal{E}} = 0.5$ (12b). When we add a recovery dynamics, we observe that at some point, the area of degraded ECM stops expanding and the porosity tends to get back to its physiological state (12c). In the fourth set of simulations, the recovery dynamics is not considered anymore but we take the natural degradation of the enzyme into account. In this case, the area of degraded ECM starts expanding then reaches its equilibrium state (12d). In the last set of simulations, all the effects are considered together (12e).

4.3 Numerical tests in 2D

The computational domain. Figure 13 shows a schematic representation of the 2D reference domain.

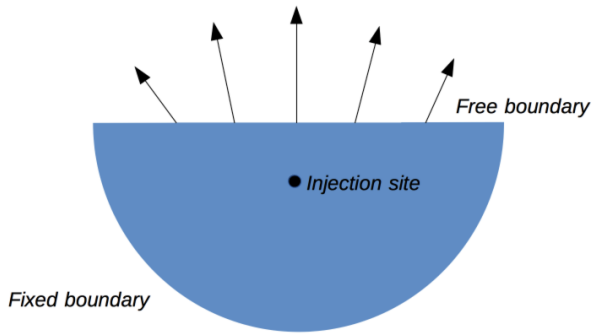

Fig. 13 Schematic representation of the 2D reference domain. As in the 1D case, the border of the domain is divided in two parts: $\Gamma = \Gamma_0 \cup \Gamma_f$. On Γ_0, Dirichlet boundary conditions are imposed, while on Γ_f, free boundary conditions are imposed.

Simulation tests. As before, we consider in this section system (54) without equation (54g) and $\overline{\gamma}$ is chosen so the initial pressure, derived from equation (62), is a constant. Parameters K, a_r and k^d_{enz} are set in order to mainly observe during the simulation time the deterioration effect of the enzyme on the ECM. This second set of simulation tests in 2D consists mainly in comparing the isotropic and transverse isotropic cases. As expected the main difference lies in the shape of the area where the ECM has been deteriorated. These 2D simulations emphasize mainly the possibility offered by the mathematical model we developed of considering anisotropic media.

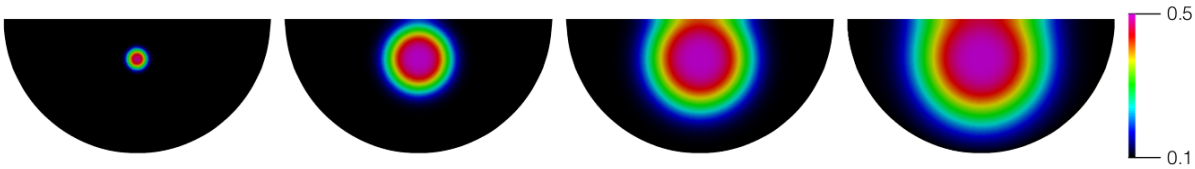

(a) Porosity at $t = 1, 10, 30, 60$ minutes in the 2D isotropic case

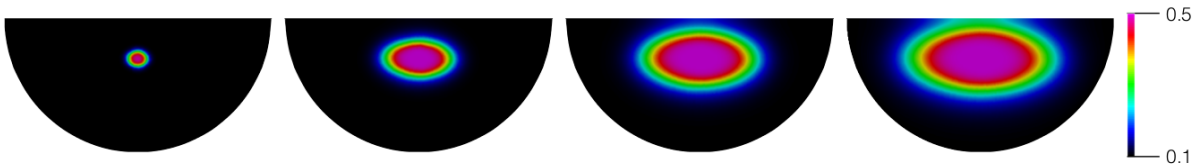

(b) Porosity at $t = 1, 20, 60, 120$ minutes in the 2D anisotropic case

Fig. 14 Porosity changes at $t = 1$ min, 10 min, 30 min and 1 hour in the 2D case for $K = 50$, $a_r = 0.0005$ and $k^d_{\text{enz}} = 0.0001$.

5 Comparison with experiments: drug penetration in solid tumors

5.1 Experimental framework

To be most effective, anticancer drugs must penetrate tumor tissue efficiently, reaching all cells in a high-enough concentration to exert a therapeutic effect. Nevertheless, the distribution of many anticancer drugs in tumor tissue is incomplete, as physiological transport barriers can strongly abate their efficiency (Minchinton and Tannock 2006; Trédan et al 2007). In particular, the composition and structure of the extracellular matrix can slow down the movement of molecules within the tumor (Netti et al 2000). Degradation of the ECM is assumed to improve the penetration of drugs. Delivery of drug to tumor cells

Table 2 Values of the model parameters in the simulations of Sections 4 and 5, except from K, a_r, k^d_{enz} otherwise specified. Parameters indexed with a * have different values in Section 5 (see Table 3).

Parameter	Symbol	Value	Unit	Reference
Typical lenght	l_0	10^{-2}	m	
Reference concentration	c_0	10^9	kg/m^3	
Density of fluid phase	ρ_f^R	10^3	kg/m^3	Yao et al (2012)
Density of solid phase	$\rho_s^{R,0}$	1.09×10^3	kg/m^3	Ward and Lieber (2005)
Specific storage coefficient	s_0	10^{-6}	Pa^{-1}	
Injected concentration	$c^{\text{enz}}_{\text{inj}}$	4×10^{-2}	U/μl	Signori et al (2001)
Diffusion coefficient of the enzyme*	D^0_{enz}	10^{-8}	m^2/s	
Permeability	κ	10^{-11}	m^{2}Pa^{-1}s^{-1}	Swartz and Fleury (2007)
Lamé first parameter	λ	7.14×10^5	Pa	Zöllner et al (2012)
Lamé second parameter	μ	1.79×10^5	Pa	Zöllner et al (2012)
Diffusion coefficient perpendicular to a fiber's axis	$D^0_{\text{enz},\perp}$	10^{-8}	m^2/s	
Diffusion coefficient parallel to a fiber's axis	$D^0_{\text{enz},//}$	$1.5 \times D^0_{\text{enz},\perp}$	-	Cleveland et al (1976)
Permeability perpendicular to a fiber's axis	$\kappa_\perp$	10^{-11}	m^{2}Pa^{-1}s^{-1}	
Permeability parallel to a fiber's axis	$\kappa_{//}$	$1.5 \times \kappa_\perp$	-	
Elastic constants (TI case)	C_{1111}	2.64×10^6	Pa	Levinson (1987)
	C_{1133}	3.39×10^6	Pa	Levinson (1987)
	C_{1313}	10^2	Pa	Levinson (1987)
	C_{3333}	4.4×10^6	Pa	Levinson (1987)

Initial values	Symbol	Initial value	Unit
Volume fraction of fluid	$\varphi_f(0,\mathbf{x}) = \varphi_f^{\text{phys}}$	0.1	-
Volume fraction of ECM	$\varphi_{\mathcal{E}}(0,\mathbf{x})$	0.4	-
Volume fraction of cells	$\varphi_e(0,\mathbf{x})$	0.5	-
Network dilatation	$\nabla \cdot \mathbf{u}(0,\mathbf{x})$	0	-
Concentration in enzyme	$h(0,\mathbf{x})$	0	Um^{-3}
Pressure	$p(0,\mathbf{x})$	0	Pa

occurs by two independent mechanisms: diffusion due to the concentration gradient and convection due to pressure gradient. It has been shown that both those mechanisms are enhanced when the tissue is previously injected or incubated with ECM degradation enzymes such as hyaluronidase and collagenase (Eikenes et al 2005, 2010, 2004). Multicellular spheroids are spherical aggregates of tumor cells that reflect many properties of solid tumors, including the development of an ECM, therefore they have been used to study the penetration of anticancer drugs into tumor tissue (Minchinton and Tannock 2006). Experimental results are consistent in showing limited drug penetration into spheroids (Sutherland et al 1979). A pretreatment with hyaluronidase or collagenase was shown to increase the diffusion coefficient of larger molecules in spheroids, and the enzymatic treatment also improved the diffusion in the case of smaller molecules in tumor tissue (Eikenes et al 2010), thereby improving the tissue sensitivity to cytotoxic drugs (St Croix et al 1998; Kohno et al 1994). Spheroids models allow to evaluate the influence of diffusion on drugs transport, but some features of solid cancer such as variable IFP and the influence of convection (which commonly occurs in the periphery of tumors) are not modeled (Minchinton and Tannock 2006). In vivo, the disorganized vascular network and the absence of functional lymphatics causes increased interstitial fluid pressure, which is uniformly elevated throughout a solid tumor and drops precipitously in the tumor periphery (Jain and Baxter 1988; Boucher et al 1990). The high IFP is a major obstacle to penetration of therapeutic molecules, as the transcapillary pressure gradient is low, and an outward interstitial flux is generated toward the periphery of the tumor due to the steep pressure gradient in the periphery of the tumor. It has been shown that hyaluronidase and collagenase reduce IFP, thereby improving the tumor uptake and distribution of molecules within solid tumors (Eikenes et al 2005; Brekken and de Lange Davies 1998). The tumor (resp. spheroid) is modeled as a sphere and consequently we chose to perform numerical simulations in axisymmetry. We use the 2D computational domain shown in Figure 19. No calibration of the parameters was done, our objective being to observe the qualitative effects of the incubation with ECM degradation enzyme of a spheroid on diffusion on one hand, and of an intratumoral injection of ECM degradation enzyme on transcapillary transport on the other hand.

5.2 Effect of an ECM degradation enzyme on diffusion of therapeutic agent

5.2.1 Boundary conditions

Define the portions of the boundary Γ_{ext}, the surface of the spheroid, and Γ_{int} the inner boundaries. To take into account the axisymmetric geometry of the domain, we choose on the internal boundaries Γ_{int} homogeneous Neumann conditions on P, h and c and we impose that the displacement will only be radial. On the surface of a spheroid, there are no contact forces and the pressure at the outer edge is the same as the pressure in the surrounding medium, that we set to be equal to P_{ext}.

$$\begin{cases} \mathbf{S}_s^E \mathbf{n} = 0 \text{ on } \Gamma_{\text{ext}}, & \mathbf{u} \cdot \mathbf{n} = 0 \text{ on } \Gamma_{\text{int}}, \quad (69a) \\ P = P_{\text{ext}} \text{ on } \Gamma_{\text{ext}}, & \nabla P \cdot \mathbf{n} = 0 \text{ on } \Gamma_{\text{int}}, \quad (69b) \end{cases}$$

During the first hour, the spheroid is incubated with the enzyme, so instead of taking a source term in equation (54d), we choose a Dirichlet boundary condition on h.

$$\begin{cases} h = \dfrac{\alpha}{c_0} c_{\text{inj}}^{\text{enz}} \text{ on } \Gamma_{\text{ext}}, & \nabla h \cdot \mathbf{n} = 0 \text{ on } \Gamma_{\text{int}}, \quad (70) \end{cases}$$

After one hour, the medium containing the enzyme is removed and a fresh medium containing the molecule of interest is added. Consequently, we choose a Dirichlet boundary condition on c and we set the outter flux of enzyme to be zero.

$$\begin{cases} \left(\mathbf{D}_{\text{enz}}^0 \nabla h + h J_{\text{enz}}\right) \cdot \mathbf{n} = 0 \text{ on } \Gamma_{\text{ext}}, & \nabla h \cdot \mathbf{n} = 0 \text{ on } \Gamma_{\text{int}}, \quad (71a) \\ c = \dfrac{\alpha}{c_0} c_{\text{inj}}^{\text{drug}} \text{ on } \Gamma_{\text{ext}}, & \nabla c \cdot \mathbf{n} = 0 \text{ on } \Gamma_{\text{int}}. \quad (71b) \end{cases}$$

After a while, the spheroid can be removed from this second medium. In this third case, we set the outter flux of enzyme and of therapeutic agent to be zero.

$$\begin{cases} \left(\mathbf{D}_{\text{enz}}^0 \nabla h + h J_{\text{enz}}\right) \cdot \mathbf{n} = 0 \text{ on } \Gamma_{\text{ext}}, & \nabla h \cdot \mathbf{n} = 0 \text{ on } \Gamma_{\text{int}}, \quad (72a) \\ \left(\mathbf{D}_{\text{drug}}^0 \nabla c + c J_{\text{drug}}\right) \cdot \mathbf{n} = 0 \text{ on } \Gamma_{\text{ext}}, & \nabla c \cdot \mathbf{n} = 0 \text{ on } \Gamma_{\text{int}}. \quad (72b) \end{cases}$$

5.2.2 Effect on porosity

As expected, the porosity remains quasi constant and equal to its initial constant value (0.1 in this case) when the spheroid is incubated in a medium with no enzyme. On the contrary, it varies when the tissue is incubated with an ECM degradation enzyme. Thus, at $t = 60$ minutes, the ECM has been degraded substantially all over the spheroid, and although the degradation of the ECM is slightly higher at the boundary, the effect is quite homogeneous (Figure 15a). As far as the total mass of fluid within the spheroid is concerned, it increases gradually while the enzyme degrades the ECM (Figure 15b).

5.2.3 Results

ECM degradation enzymes such as collagenase and hyaluronidase were shown to increase the diffusion of macromolecules in spheroid and in tumor tissue, with a greater impact witnessed in the case of collagenase compared to hyaluronidase (Eikenes et al 2010). We performed simulations to evaluate the effect of an incubation of a spheroid with enzyme on the distribution of drugs with a low coefficient of diffusion ($D_{\text{drug}}^0 = 10^{-9}$ ui), such as the one of a macromolecule. We simulate the incubation during 5 minutes with a therapeutic agent one hour after the incubation with collagenase and we observed the behavior of the drug concentration for ten minutes, including the 5 minutes of incubation. It can be observed that the area where the drug is present above a certain minimum concentration is wider when the spheroid was previously incubated with collagenase (Figure 16).
We then performed simulations to evaluate the effect of an incubation of a spheroid with enzyme on the distribution of drugs with an higher coefficient of diffusion ($D_{\text{drug}}^0 = 10^{-6}$ ui), such as the one of a small molecule. In this case, the whole domain is affected with or without pretreatment, but the degraded

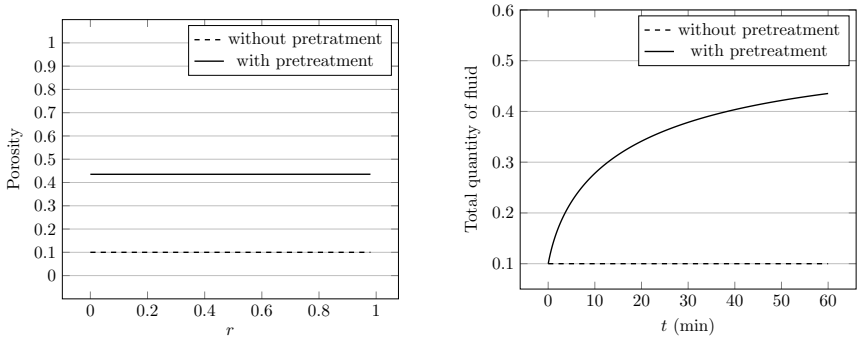

(a) Porosity versus radial position at the end of the incubation phase.

(b) Quantity of fluid in the tissue versus time.

Fig. 15 Effect on the porosity of a tissue incubated with collagenase (20 U) during 60 minutes compared to incubated with a saline solution (0 U).

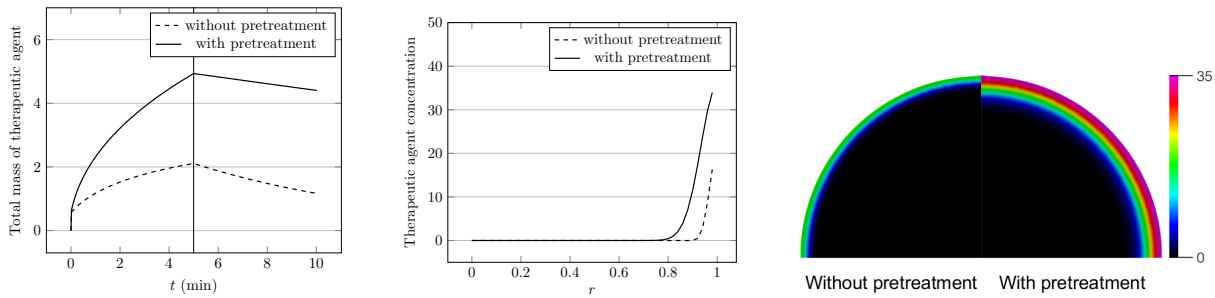

(a) Drug's total mass in the tissue versus time.

(b) Drug's concentration plotted versus the postion in the tumor at time $t = 10$ minutes.

(c) 2D-drug's concentration in the tumor at time $t = 10$ minutes.

Fig. 16 Numerical results for a therapeutic agent with a low coefficient of diffusion incubated during 5 minutes.

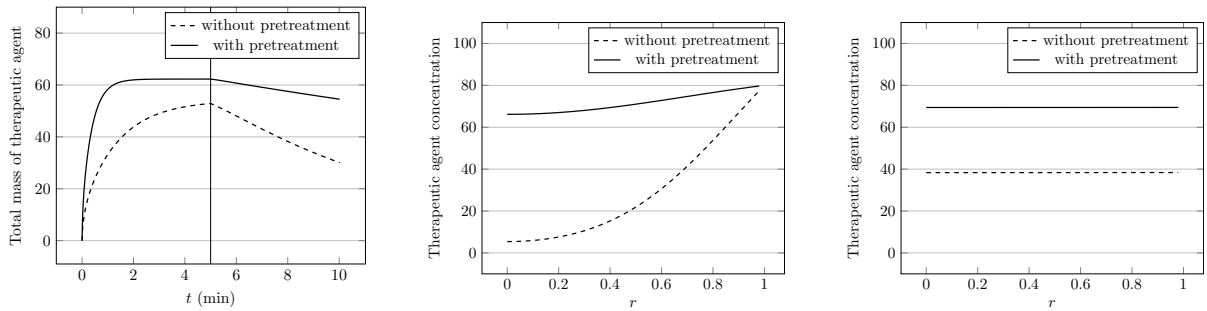

(a) Drug's total mass in the tissue versus time.

(b) Drug's concentration plotted versus the postion in the tumor at time $t = 1$ minute.

(c) Drug's concentration plotted versus the postion in the tumor at time $t = 10$ minutes.

Fig. 17 Numerical results for a therapeutic agent with an higher coefficient of diffusion incubated during 5 minutes.

ECM has two main effects: the drug reaches the whole domain faster, and naturally degrades slower which results in a higher concentration of drug throughout the tissue after 10 minutes (Figure 17).
We finally performed simulations with a quite low coefficient of diffusion ($D^0_{\text{drug}} = 10^{-8}$ ui), but for a tissue incubated longer (15 minutes) and we waited 15 more minutes to look at the drug's distribution. In this case, the result is qualitatively in agreement with the experiments developed by Kohno et al (1994) (cf Figure 3): with an enzyme pretreatment, the drug distribution after 30 minutes (including 15 minutes of incubation) is way better than if the tissue was not pretreated (Figure 18). The drug is not only present all over the tissue, its concentration is also higher, improving thus the chances of uptake by the cells.

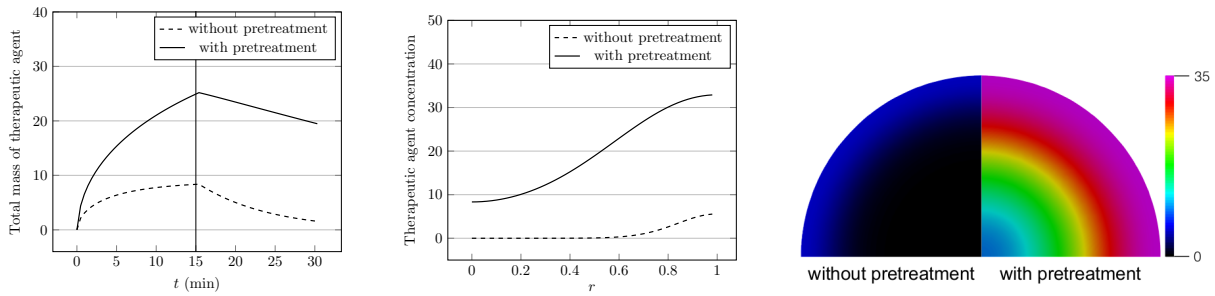

(a) Drug's total mass in the tissue versus time.

(b) Drug's concentration plotted versus the postion in the tumor at time $t = 30$ minutes.

(c) 2D-drug's concentration in the tumor at time $t = 30$ minutes.

Fig. 18 Numerical results for a therapeutic agent with a quite low coefficient of diffusion incubated during 15 minutes.

In the specific framework of an injection of DNA plasmids, a question of interest would be to determine when to do electrotransfer. If the best moment is when the area where the DNA plasmids concentration is above a certain minimum concentration is the widest, then the model, rightfully calibrated, could allow to calculate this optimized time.

Table 3 Values of the specific model parameters in the simulations of Section 5. All other parameters are taken from Table 2.

Parameter	Symbol	Value	Unit	Reference
Diffusion coefficient of the enzyme	D^0_{enz}	10^{-4}	m^2/s	
Diffusion coefficient of the therapeutic agent	D^0_{drug}	10^{-9}, 10^{-6}, 10^{-8}	m^2/s	
Starling's coefficient	γ	5×10^{-5}	$\text{Pa}^{-1}\text{s}^{-1}$	Soltani and Chen (2012)
Fluid/solute coefficient	γ_c	0.9	-	Baxter and Jain (1989)
Measure of treatment efficacity	K	10^{-14}	$\text{m}^3\text{s}^{-1}\text{U}^{-1}$	
Recovery coefficient	a_r	5×10^{-4}	s^{-1}	
Degradation rate of the enzyme	k^d_{enz}	1×10^{-4}	s^{-1}	
Degradation rate of the therapeutic agent	k^d_{drug}	2×10^{-4}	s^{-1}	
Driving pressure	P_v	10^{-1}	Pa	

Initial values	Symbol	Initial value	Unit
Concentration in drug	$c(0, \mathbf{x})$	0	kg m^{-3}
Pressure incubation case	$p(0, \mathbf{x})$	0	Pa

5.3 Effect of an ECM degradation enzyme on transcapillary transport of therapeutic agent

5.3.1 Boundary conditions

Define the portions of the boundary Γ_{ext}, the surface of the tumor, and Γ_{int} the inner boundaries. On the surface of an isolated tumor, there are no contact forces and the pressure at the outer edge is the same as the pressure in the surrounding tissue, that we set to zero. On the concentration of the injected species, we assume that their flux is zero on Γ_{ext}. To take into account the axisymmetric geometry of the domain, we choose on the internal boundaries Γ_{int} homogeneous Neumann conditions on P, h and c and we impose that the displacement will only be radial.

$$\begin{cases} \mathbf{S}^E_s\,\mathbf{n} = 0 \text{ on } \Gamma_{\text{ext}}, & \mathbf{u}\cdot\mathbf{n} = 0 \text{ on } \Gamma_{\text{int}}, \quad (73a)\\ P = 0 \text{ on } \Gamma_{\text{ext}}, & \nabla P\cdot\mathbf{n} = 0 \text{ on } \Gamma_{\text{int}}, \quad (73b)\\ \left(\mathbf{D}^0_{\text{enz}}\nabla h + hJ_{\text{enz}}\right)\cdot\mathbf{n} = 0 \text{ on } \Gamma_{\text{ext}}, & \nabla h\cdot\mathbf{n} = 0 \text{ on } \Gamma_{\text{int}}, \quad (73c)\\ \left(\mathbf{D}^0_{\text{drug}}\nabla c + cJ_{\text{drug}}\right)\cdot\mathbf{n} = 0 \text{ on } \Gamma_{\text{ext}}, & \nabla c\cdot\mathbf{n} = 0 \text{ on } \Gamma_{\text{int}}. \quad (73d)\end{cases}$$

5.3.2 Initial pressure profile

In the simulations, $\overline{P_v}$ and $\overline{\gamma}$ are chosen so the initial pressure profile, derived from equation (62), fits the type of IFP profile observed in tumors (Figure 19).

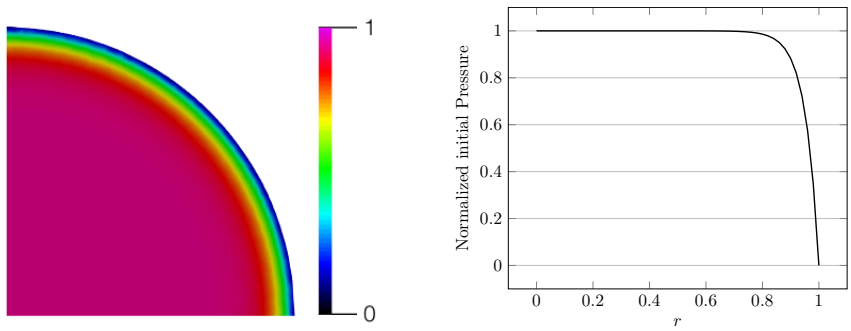

(a) Normalized 2D-pressure in the tumor before the experiment.

(b) Normalized pressure in the tumor before the experiment versus position.

Fig. 19 Initial normalized pressure profile. This type of steep profile is in agreement with previous studies (Baxter and Jain 1989).

5.3.3 Effect on porosity

As observed in Section 4.2, the porosity remains quasi constant when only a saline solution is injected. On the contrary, it varies when the tissue is injected with an ECM degradation enzyme. At $t = 60$ minutes, we observe that without enzyme, the porosity is equal to its initial constant value (0.1 in this case) while in presence of enzyme, the ECM has been degraded substantially all over the tissue. Although the degradation of the ECM is the slightly higher in the vicinity of the injection point, the effect is quite homogeneous. As expected, the total mass of fluid within the tissue increases gradually while the enzyme degrades the ECM.

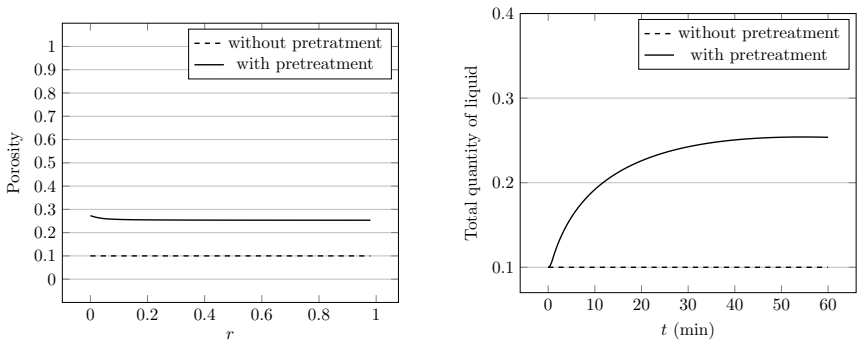

(a) Porosity versus radial position 60 minutes after the injection.

(b) Quantity of fluid in the tissue versus time.

Fig. 20 Effect on the porosity of a tumor injected with hyaluronidase (1500 U) compared to injected with a saline solution (0 U).

5.3.4 Effect on the IFP

The effect of hyaluronidase on IFP was demonstrated experimentally by Eikenes et al (2005) and Brekken and de Lange Davies (1998). Intratumoral injection of hyaluronidase in tumors reduced IFP in a dose-

dependent manner up to a maximum reduction. However, by increasing the dose further, IFP was reduced to a lesser extent. An initial increase in IFP was observed, explained by the increase in the volume and compression of the tissue at the moment of the intratumoral injection.

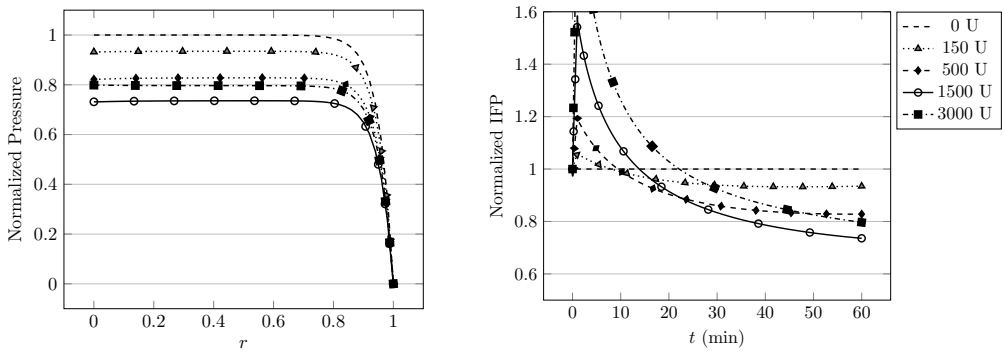

(a) Normalized IFP versus position at time $t = 60$ minutes.

(b) Normalized IFP versus time.

Fig. 21 Effect on the normalized interstitial fluid pressure of a tumor injected with hyaluronidase (500 U, 1500 U, 3000 U) compared to injected with a saline solution.

The simulation reproduces the three main effects observed in the experiments: an initial increase in IFP due to the intratumoral injection, the fact that IFP reaches a reduced value after some time and finally the non-linear behavior regarding the concentration.

5.3.5 Results

It was shown that both hyaluronidase and collagenase increase convection by inducing transcapillary pressure gradients in human osteosarcoma xenografts (Eikenes et al 2005, 2004). We have seen previously that an injection of enzyme has an effect on the IFP, inducing a transcapillary pressure gradient in a dose-dependent manner up to a maximum reduction. Increasing the dose further, IFP is reduced to a lesser extent. This reduction was shown to improve both the distribution and the uptake of drugs in tumors (Eikenes et al 2005). In this section, we focus on the distribution of drugs. We simulate an injection during 1 minute of a therapeutic agent one hour after the injection of enzyme and we observed the behavior of the drug's concentration for ten minutes, including during the injection. For all simulations, the same value of $c_v(t, \mathbf{x}) = \chi_{\{0 \leq t \leq 1\,\mathrm{min}\}}(t)\, c_v$ is taken while different values of $c_{\mathrm{inj}}^{\mathrm{enz}}$ previously injected are considered. For a drug with a low coefficient of diffusion, such as the one of a macromolecule, several features are observed. First, the total mass of therapeutic agent that actually reaches the tumor by transcapillary transport varies with the concentration of enzyme previously injected (Figure 22a). Second, while without enzyme the therapeutic agent only penetrates the periphery of the tumor, we observe that with a pretreatment, the therapeutic agent is present all over the tumor (Figure 22b). Finally, the same non-linear behavior regarding the concentration of enzyme previously injected is observed. In particular, if the concentration of enzyme is too high, as the pressure is reduced to a lesser extent, the drug's penetration in the tumor by transcapillary transport is also reduced.
For a drug with an higher coefficient of diffusion, such as the one of a smaller molecule, the transcapillary transport in the tumor is also improved, but the main features of interest are different. In particular, as the drug reaches the whole tumor mainly by diffusion in any case, the contributions of the pretreatment of the tumor with an ECM degradation enzyme are the same as the ones developed in the previous subsection concerning spheroids. In particular, it is when the concentration of enzyme previously injected is the highest that the drug reaches homogeneously the tumor the fastest and that the natural degradation process is slowed the most. Nevertheless, the total mass of therapeutic agent that actually reaches the tumor by transcapillary transport is consistent with the reduction of IFP in the same non-linear behavior regarding the concentration of enzyme, and consequently, at $t = 10$ minutes, the best configuration is also obtained for the concentration of enzyme that induces the highest reduction in IFP.

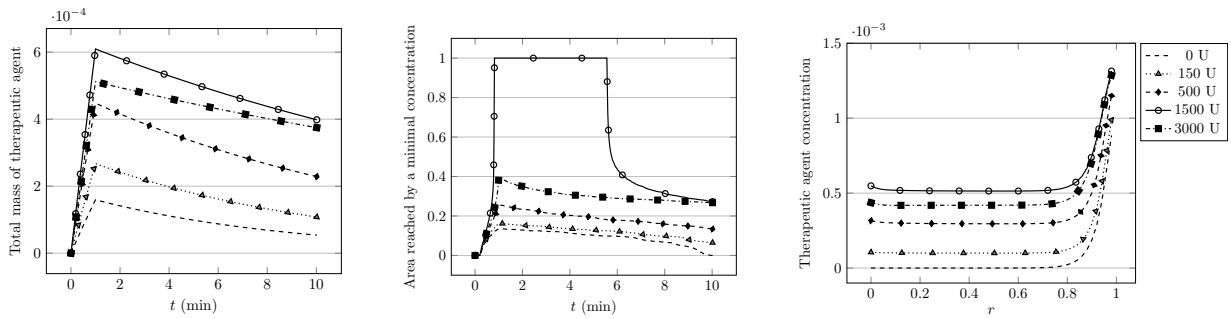

(a) Drug's total mass in the tissue versus time.

(b) Normalized area reached by a minimal concentration of therapeutic agent versus time.

(c) Drug's concentration plotted versus the postion in the tumor at time $t = 5$ minutes.

Fig. 22 Numerical results for a therapeutic agent with a low coefficient of diffusion injected intravenously.

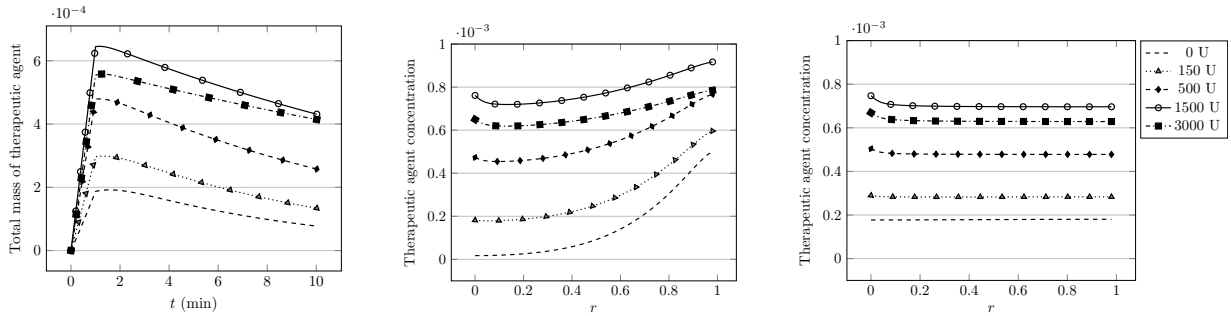

(a) Drug's total mass in the tissue versus time.

(b) Drug's concentration plotted versus the postion in the tumor at time $t = 1$ minute.

(c) Drug's concentration plotted versus the postion in the tumor at time $t = 5$ minutes.

Fig. 23 Numerical results for a therapeutic agent with an higher coefficient of diffusion injected intravenously.

The distribution of the drug into the tissue is directly correlated with the transcapillary pressure gradient created by the hyaluronidase injected. In particular, it is for the hyaluronidase's concentration value for which the maximum pressure reduction is obtained that we obtained the best distribution profile. Increasing the dose further, the pressure is reduced to a lesser extent and the consequence on the distribution of drug is that the area where the concentration of therapeutic agent is above a minimum concentration value is smaller. This result is in agreement with the experiments described by Eikenes et al (2005) where hyaluronidase was shown to greatly improve the distribution of doxorubicin. To go further and consider the possibility of using the model as a strategy to optimize drug delivery, we would need more experimental data to calibrate the model parameters.

6 Conclusion

In this paper we developed a novel mathematical formulation to describe the effect of an ECM degradation enzyme on a soft biological tissue. The principal novelty of our contribution is the development of a model based on the use of Partial Differential Equations (PDEs) that incorporates the effect of an ECM degradation enzyme within the general and well established framework of poroelastic theory of mixtures. Specifically, where usually the fraction volumes of the different phases are assumed to be constants, we derive evolutive equations to describe them. Having defined the possible interactions between phases, our approach consists in deriving a system of conservation laws (mass and linear momentum) for the phases and components of the mixture that includes the enzyme concentration as main determinant of porosity evolution. The next step was to develop a numerical approximation of the mathematical model introduced in the article. As the medium is assumed to be poroelastic, it can undergo some deformation and potentially change of shape if a boundary condition is applied on stress. It was necessary to formulate

our model in a reference fixed domain before developing a computational algorithm to approximate the system's solution. Below we address the more significant outcomes of the conducted simulations.

1. The illustrated numerical tests conducted in 1D indicate the role of each new parameter on the porosity evolution.
2. The illustrated numerical results in 2D can describe a well-known principle of prefential flow in the direction of the fiber tracts in the context of a transverse anisotropic media.
3. Model simulations indicate that an intratumoral injection of hyaluronidase results in a reduction of the IFP in a dose-dependent manner up to a maximum reduction, and that once that maximum reduction is achieved, a further increase of the dose results in a smaller reduction. This finding represents a favorable result from the experimentalist point of view, because it is in agreement with several observations previously reported.
4. The injection of an ECM degradation enzyme was also shown to enhance distribution, by improving diffusion and/or convection, of drug throughout the tissue. This outcome reinforces the idea that, used in medicine, these enzymes can improve a treatment by widening its field of action.

Further research effort will be devoted to calibrating the model parameters with additional experimental data and to considering domains with more complex 3D geometries. To this end one can cite the preliminary works presented in Deville's thesis (Deville 2017) on the numerical nonlinear optimization of the model by mean of kriging method. A forthcoming effort will also be made to rightfully coupled this model with an electrical model in order to explain and quantify the uptake of DNA plasmids observed by Signori et al (2001).

Acknowledgements The authors thank Professor E. Signori for her advices and fruitful discussions on the experimental features of drug injection in tumor and muscles.
M.D. is partly granted by "Université Franco-Italienne", project VINCI C2-25. M.D. and C.P. are partly granted by the Plan Cancer DYNAMO (Inserm 9749) and Plan Cancer NUMEP (Inserm 11099). This study has been carried out within the scope of the European Associate Lab EBAM, and the Inria Associate Team Num4SEP.

Bibliography

Akerstrom T, Vedel K, Needham J, Hojman P (2015) Optimizing hyaluronidase dose and plasmid DNA delivery greatly improves gene electrotransfer efficiency in rat skeletal muscle. Biochemistry and Biophysics Reports

Alì G, Furuholt V, Natalini R, Torcicollo I (2007) A mathematical model of sulphite chemical aggression of limestones with high permeability. Part I. Modeling and qualitative analysis. Transport in Porous Media 69:109–122

Altrock PM, Liu LL, Michor F (2015) The mathematics of cancer: integrating quantitative models. Nature Reviews Cancer 15(12):730–745

Ambrosi D (2002) Infiltration through deformable porous media. ZAMM Zeitschrift für Angewandte Mathematik und Mechanik Journal of Applied Mathematics and Mechanics 82(2):115–124

Ambrosi D, Lancellotta R, Preziosi L (2002) Mathematical models for soil consolidation problems : a state of the art report. Chapter 6 of Modeling and Mechanics of Granular and Porous Materials pp 159–180

André F, Mir LM (2004) DNA electrotransfer: its principles and an updated review of its therapeutic applications. Gene therapy 11 Suppl 1:S33–42

Astanin S, Preziosi L (2008) Selected Topics in Cancer Modeling: Genesis, Evolution, Immune Competition, and Therapy, Birkhäuser Boston, chap Multiphase Models of Tumour Growth, pp 1–31

Bae YH, Mrsny RJ, Park K (2013) Cancer targeted drug delivery

Barry SI, Aldis GK (1991) Unsteady-Flow Induced Deformation of Porous Materials. International Journal of Non-Linear Mechanics 26(5):687–699

Barry SI, Mercer GN (1999) Flow and deformation in poroelasticity. I. Unusual exact solutions. Mathematical and Computer Modelling 30(9-10):23–29

Basser PJ (1992) Interstitial pressure, volume, and flow during infusion into brain tissue. Microvascular research 44(2):143–165

Batra RC (1998) Linear constitutive relations in isotropic finite elasticity. Journal of Elasticity The Physical and Mathematical Science of Solids 51(3):243–245

Baxter LT, Jain RK (1989) Transport of fluid and macromolecules in tumors. I. Role of interstitial pressure and convection. Microvascular research

Bear J, Bachmat Y (1990) Introduction to Modeling of Transport Phenomena in Porous Media. Kluwer Academic Publishers

Biot MA (1941) General theory of three-dimensional consolidation. Journal of applied physics 12(2):155

Bottaro A, Ansaldi T (2012) On the infusion of a therapeutic agent into a solid tumor modeled as a poroelastic medium. Journal of biomechanical engineering 134(8):084,501

Boucher Y, Baxter LT, Jain RK (1990) Interstitial Pressure Gradients in Tissue-isolated and Subcutaneous Tumors: Implications for Therapy. Cancer research 50(15):4478–4484

Bowen RM (1980) Incompressible porous media models by use of the theory of mixtures. International Journal of Engineering Science 18(9):1129–1148

Brekken C, de Lange Davies C (1998) Hyaluronidase reduces the interstitial fluid pressure in solid tumours in a non-linear concentration-dependent manner. Cancer letters 131(1):65–70
Buhren BA, Schrumpf H, Hoff NP, Bölke E, Hilton S, Gerber PA (2016) Hyaluronidase: from clinical applications to molecular and cellular mechanisms. European journal of medical research 21(1):5
Bureau MF, Naimi S, Ibad RT, Seguin J (2004) Intramuscular plasmid DNA electrotransfer: biodistribution and degradation. Biochimica et Biophysica Acta (BBA)
Chapelle D, Moireau P (2014) General coupling of porous flows and hyperelastic formulations. from thermodynamics principles to energy balance and compatible time schemes. European Journal of Mechanics - B/Fluids 46(Supplement C):82 – 96
Chaplain MAJ, Graziano L, Preziosi L (2006) Mathematical modelling of the loss of tissue compression responsiveness and its role in solid tumour development. Mathematical medicine and biology : a journal of the IMA 23(3):197–229
Chen Z, Huan G, Ma Y (2006) Computational methods for multiphase flows in porous media. Computational Science & Engineering, Society for Industrial and Applied Mathematics (SIAM), Philadelphia, PA
Choi IK, Strauss R, Richter M, Yun CO, Lieber A (2013) Strategies to increase drug penetration in solid tumors. Frontiers in oncology 3:193
Cleveland GG, Chang DC, Hazlewood CF, Rorschach HE (1976) Nuclear magnetic resonance measurement of skeletal muscle: anisotrophy of the diffusion coefficient of the intracellular water. Biophysical journal 16(9):1043–1053
Damon BM, Buck A, Ding Z (2011) Diffusion-tensor mri-based skeletal muscle fiber tracking. Imaging in medicine
Delingette H (1998) Toward realistic soft-tissue modeling in medical simulation. In: Proceedings of the IEEE
Deville M (2017) Mathematical modeling of enhanced drug delivery by mean of electroporation or enzymatic treatment. Thesis, Université de Bordeaux
Eikenes L, Bruland ØS, Brekken C, Davies CdL (2004) Collagenase increases the transcapillary pressure gradient and improves the uptake and distribution of monoclonal antibodies in human osteosarcoma xenografts. Cancer research 64(14):4768–4773
Eikenes L, Tari M, Tufto I, Bruland ØS, de Lange Davies C (2005) Hyaluronidase induces a transcapillary pressure gradient and improves the distribution and uptake of liposomal doxorubicin (Caelyx) in human osteosarcoma xenografts. British journal of cancer 93(1):81–88
Eikenes L, Tufto I, Schnell EA, Bjørkøy A, De Lange Davies C (2010) Effect of collagenase and hyaluronidase on free and anomalous diffusion in multicellular spheroids and xenografts. Anticancer research 30(2):359–368
Escoffre JM, Teissie J, Rols MP (2010) Gene transfer: how can the biological barriers be overcome? The Journal of membrane biology 236(1):61–74
Feng X, Ge Z, Li Y (2014) Multiphysics Finite Element Methods for a Poroelasticity Model. arXivorg 1411.7464
Frantz C, Stewart KM, Weaver VM (2010) The extracellular matrix at a glance. Journal of cell science 123(Pt 24):4195–4200
Fung YC (1981) Biomechanics: mechanical properties of living tissues
Fusi L, Farina A, Ambrosi D (2006) Mathematical Modeling of a Solid–Liquid Mixture with Mass Exchange Between Constituents. Mathematics and Mechanics of Solids 11(6):575–595
Ganesh S, Gonzalez-Edick M, Gibbons D, Van Roey M, Jooss K (2008) Intratumoral coadministration of hyaluronidase enzyme and oncolytic adenoviruses enhances virus potency in metastatic tumor models. Clinical cancer research : an official journal of the American Association for Cancer Research 14(12):3933–3941
Girish KS, Kemparaju K (2007) The magic glue hyaluronan and its eraser hyaluronidase: a biological overview. Life sciences 80(21):1921–1943
Giverso C, Scianna M, Grillo A (2015) Growing avascular tumours as elasto-plastic bodies by the theory of evolving natural configurations. Mechanics Research Communications 68(Supplement C):31 – 39, bruno Boley 90th Anniversary Issue
Happel MFK, Niekisch H, Castiblanco Rivera LL, Ohl FW, Deliano M, Frischknecht R (2014) Enhanced cognitive flexibility in reversal learning induced by removal of the extracellular matrix in auditory cortex. Proceedings of the National Academy of Sciences of the United States of America 111(7):2800–2805
Hecht F (2012) New development in FreeFem++. Journal of numerical mathematics
Jain RK, Baxter LT (1988) Mechanisms of Heterogeneous Distribution of Monoclonal Antibodies and Other Macromolecules in Tumors: Significance of Elevated Interstitial Pressure. Cancer research 48(24 Part 1):7022–7032
Juhlin L (1956) Reconstitution of dermal connective tissue barrier after testicular or bacterial hyaluronidase. Acta Pharmacologica et Toxicologica 12(1):96–108
Juliano R (2007) Challenges to macromolecular drug delivery. Biochemical Society transactions 35(Pt 1):41–43
Kohno N, Ohnuma T, Truog P (1994) Effects of hyaluronidase on doxorubicin penetration into squamous carcinoma multicellular tumor spheroids and its cell lethality. Journal of cancer research and clinical oncology 120(5):293–297
Lang GE, Vella D, Waters SL, Goriely A (2016) Mathematical modelling of blood-brain barrier failure and oedema. Mathematical medicine and biology : a journal of the IMA
Leguèbe M, Notarangelo M, Twarogowska M, Natalini R, Poignard C (2017) Mathematical model for transport of dna plasmids from the external medium up to the nucleus by electroporation. Mathematical Biosciences 285(Supplement C):1 – 13
Lemon G, King JR, Byrne HM, Jensen OE, Shakesheff KM (2006) Mathematical modelling of engineered tissue growth using a multiphase porous flow mixture theory. Journal of Mathematical Biology 52(5):571–594
Levinson SF (1987) Ultrasound propagation in anisotropic soft tissues: the application of linear elastic theory. Journal of biomechanics 20(3):251–260
Lokeshwar VB, Selzer MG (2008) Hyalurondiase: Both a tumor promoter and suppressor. Seminars in Cancer Biology 18(4):281 – 287, hyaluronan in Cancer Biology
Magzoub M, Jin S, Verkman AS (2008) Enhanced macromolecule diffusion deep in tumors after enzymatic digestion of extracellular matrix collagen and its associated proteoglycan decorin. FASEB journal : official publication of the Federation of American Societies for Experimental Biology 22(1):276–284
McAtee CO, Barycki JJ, Simpson MA (2014) Chapter one - emerging roles for hyaluronidase in cancer metastasis and therapy. In: Simpson MA, Heldin P (eds) Hyaluronan Signaling and Turnover, Advances in Cancer Research, vol 123,

Academic Press, pp 1 – 34
Minchinton AI, Tannock IF (2006) Drug penetration in solid tumours. Nature Reviews Cancer
Mow VC, Holmes MH, Lai WM (1984) Fluid transport and mechanical properties of articular cartilage: a review. Journal of biomechanics 17(5):377–394
Murad MA, Loula AFD (1992) Improved accuracy in finite element analysis of Biot's consolidation problem. Computer Methods in Applied Mechanics and Engineering 95(3):359–382
Murad MA, Loula AFD (1994) On stability and convergence of finite element approximations of Biot's consolidation problem. International Journal for Numerical Methods in Engineering 37(4):645–667
Namazi H, Kulish VV, Wong A, Nazeri S (2016) Mathematical Based Calculation of Drug Penetration Depth in Solid Tumors. BioMed research international 2016:8437,247
Netti PA, Baxter LT, Boucher Y, Skalak R, Jain RK (1997) Macro- and microscopic fluid transport in living tissues: Application to solid tumors. AIChE Journal 43(3):818–834
Netti PA, Berk DA, Swartz MA, Grodzinsky AJ, Jain RK (2000) Role of extracellular matrix assembly in interstitial transport in solid tumors. Cancer research 60(9):2497–2503
Phillips PJ, Wheeler MF (2009) Overcoming the problem of locking in linear elasticity and poroelasticity: an heuristic approach. Computational Geosciences
Pietras K, Östman A, Sjöquist M, Buchdunger E, Reed RK, Heldin CH, Rubin K (2001) Inhibition of platelet-derived growth factor receptors reduces interstitial hypertension and increases transcapillary transport in tumors. Cancer research 61(7):2929–2934
Preziosi L, Tosin A (2008) Multiphase modelling of tumour growth and extracellular matrix interaction: mathematical tools and applications. Journal of Mathematical Biology 58(4-5):625–656
Radu FA, Pop IS, Muntean A, Berre I (2014) Simulation of reactive flow in porous media with variable porosity as appears when modelling concrete carbonation. In: 11th World Congress on Computational Mechanics (WCCM XI), 5th European Conference on Computational Mechanics (ECCM V), 6th European Conference on Computational Fluid Dynamics (ECFD VI), Barcelona, Spain
Rosler J, Harders H, Baker M (2007) Mechanical behaviour of engineering materials
Royer D, Gennisson JL, Deffieux T, Tanter M (2011) On the elasticity of transverse isotropic soft tissues (L). The Journal of the Acoustical Society of America 129(5):2757–5
Sacco R, Causin P, Lelli C, Raimondi MT (2017) A poroelastic mixture model of mechanobiological processes in biomass growth: theory and application to tissue engineering. Meccanica 52(14):3273–3297
Schertzer JD, Plant DR, Lynch GS (2006) Optimizing plasmid-based gene transfer for investigating skeletal muscle structure and function. Molecular Therapy 13(4)
Signori E, Wells K, Fazio V, Wells D (2001) Optimisation of electrotransfer of plasmid into skeletal muscle by pretreatment with hyaluronidase - increased expression with reduced muscle damage. Gene Therapy 8:1264–1270
Soltani M, Chen P (2012) Effect of tumor shape and size on drug delivery to solid tumors. Journal of biological engineering
Spiegelman M (1993a) Flow in deformable porous media. Part 1 Simple analysis. Journal of Fluid Mechanics 247(-1):17–38
Spiegelman M (1993b) Flow in deformable porous media. Part 2 Numerical analysis – the relationship between shock waves and solitary waves. Journal of Fluid Mechanics 247(-1):39–63
St Croix B, Man S, Kerbel RS (1998) Reversal of intrinsic and acquired forms of drug resistance by hyaluronidase treatment of solid tumors. Cancer letters 131(1):35–44
Støverud KH, Darcis M, Helmig R, Hassanizadeh SM (2011) Modeling Concentration Distribution and Deformation During Convection-Enhanced Drug Delivery into Brain Tissue. Transport in Porous Media 92(1):119–143
Sutherland RM, Eddy HA, Bareham B, Reich K, Vanantwerp D (1979) Resistance to adriamycin in multicellular spheroids. International journal of radiation oncology, biology, physics 5(8):1225–1230
Swartz MA, Fleury ME (2007) Interstitial flow and its effects in soft tissues. Annual review of biomedical engineering 9:229–256
Trédan O, Galmarini CM, Patel K, Tannock IF (2007) Drug resistance and the solid tumor microenvironment. Journal of the National Cancer Institute 99(19):1441–1454
Ward SR, Lieber RL (2005) Density and hydration of fresh and fixed human skeletal muscle. Journal of biomechanics 38(11):2317–2320
Whatcott CJ, Han H, Posner RG, Hostetter G, Von Hoff DD (2011) Targeting the tumor microenvironment in cancer: why hyaluronidase deserves a second look. Cancer discovery 1(4):291–296
Wolff JA, Malone RW, Williams P, Chong W, Acsadi G, Jani A, Felgner PL (1990) Direct gene transfer into mouse muscle in vivo. Science (New York, NY) 247(4949 Pt 1):1465–1468
Wu L, Ding J (2005) Effects of porosity and pore size on in vitro degradation of three-dimensional porous poly (D, L-lactide-co-glycolide) scaffolds for tissue engineering. Journal of Biomedical Materials Research Part A
Yao W, Li Y, Ding G (2012) Interstitial fluid flow: the mechanical environment of cells and foundation of meridians. Evidence-based complementary and alternative medicine : eCAM 2012:853,516
Zöllner AM, Abilez OJ, Böl M, Kuhl E (2012) Stretching skeletal muscle: chronic muscle lengthening through sarcomerogenesis. PloS one 7(10):e45,661

Appendix A Formulation of the model in Ω_0 in the general case

The calculus in the general case gives the final system of equations (76). Recall that matrix B is defined as the inverse of matrix A given by (46). As,

$$(B^{-1})_{i,j} = A_{i,j} = \left(\frac{\partial \Phi(t,\mathbf{X})}{\partial \mathbf{X}}\right)_{i,j} = \delta_{ij} + \frac{\partial u_i}{\partial X_j}(t,\mathbf{X}) = \delta_{ij} + \frac{\partial \overline{u}_i}{\partial \overline{\mathbf{X}}_j}(\overline{t},\overline{\mathbf{X}}), \tag{74}$$

we kept the notation B to refer to $B(\overline{\mathbf{u}})$ in system (76). Note that we equally dropped bars on the dimensionless variables but kept them on the dimensionless parameters. Let us denote

$$J^B_{\text{enz}} = \frac{1}{f}\overline{\boldsymbol{\kappa}}\, B\nabla P - \overline{\mathbf{D}^0_{\text{enz}}} B\nabla f \qquad \text{and} \qquad J^B_{\text{drug}} = \frac{1}{f}\overline{\boldsymbol{\kappa}}\, B\nabla P - \overline{\mathbf{D}^0_{\text{drug}}} B\nabla f. \tag{75}$$

The equivalent system in Ω_0 in dimensionless form reads

$$\begin{cases} g_{\mathcal{E}} + g_{\mathcal{C}} + f = 1, & \text{(76a)} \\ \boldsymbol{\nabla}\cdot\left((g_{\mathcal{E}} + g_{\mathcal{C}})\dfrac{1}{J}B^{-1}\overline{\mathbf{S}^E_s}B^{-T}\right) = \nabla P, & \text{(76b)} \\ (g_{\mathcal{E}} + g_{\mathcal{C}})\overline{s_0}\dfrac{\partial P}{\partial t} - B\nabla\cdot(\overline{\boldsymbol{\kappa}}B\nabla P) = \alpha Q^{\text{tot}}_{\text{inj}} + \overline{\gamma}(\overline{P_v} - P) - B\nabla\cdot\left(\dfrac{\partial \mathbf{u}}{\partial t}\right) & \\ \qquad\qquad + \left(1 - \dfrac{\rho^{R,0}_s}{\rho^R_f}\right) g_{\mathcal{E}}(-\overline{K}h + \overline{a_r}\,(f - f^0)), & \text{(76c)} \\ \dfrac{\partial h}{\partial t} = B\nabla\cdot\left(f\overline{\mathbf{D}^0_{\text{enz}}}B\nabla h + hJ^B_{\text{enz}}\right) - \left(\dfrac{\overline{k^d_{\text{enz}}}}{f} + B\nabla\cdot\left(\dfrac{\partial \mathbf{u}}{\partial t}\right)\right)h + \dfrac{\alpha\mathcal{S}_{\text{enz}}}{c_0}, & \text{(76d)} \\ \dfrac{\partial g_{\mathcal{C}}}{\partial t} + g_{\mathcal{C}}\left(\overline{s_0}\dfrac{\partial P}{\partial t} + B\boldsymbol{\nabla}\cdot\left(\dfrac{\partial \mathbf{u}}{\partial t}\right)\right) = 0, & \text{(76e)} \\ \dfrac{\partial g_{\mathcal{E}}}{\partial t} + g_{\mathcal{E}}\left(\overline{s_0}\dfrac{\partial P}{\partial t} + B\boldsymbol{\nabla}\cdot\left(\dfrac{\partial \mathbf{u}}{\partial t}\right)\right) = g_{\mathcal{E}}(-\overline{K}h + \overline{a_r}\,(f - f^0)), & \text{(76f)} \\ \dfrac{\partial c}{\partial t} = B\nabla\cdot\left(f\overline{\mathbf{D}^0_{\text{drug}}}B\nabla c + cJ^B_{\text{drug}}\right) - \left(\dfrac{\overline{k^d_{\text{drug}}}}{f} + B\nabla\cdot\left(\dfrac{\partial \mathbf{u}}{\partial t}\right)\right)c + \dfrac{\alpha\mathcal{S}_{\text{drug}}}{c_0}, & \text{(76g)} \end{cases}$$

where we get (76a) from Assumption 1, (76b) from Equation (20), (76c) from (15), (76d) from (24), (76g) from (28), (76f) from (13a) and (76e) from (13b), using (50), (51) and (52).